Correlations of Horizontally Oriented Ice and Precipitation in Marine Midlatitude Clouds using Collocated A-Train Observations

---

A Thesis
Presented to
The College of Letters and Sciences
The University of Wisconsin - Madison

In Partial Fulfillment
of the Requirements for the Degree
Master of Science

Alexa Deborah Ross

August 2015

Approved for the College
(Atmospheric, Oceanic, and Space Sciences)

Steven Ackerman	Grant Petty	Tristan L'Ecuyer

Acknowledgements

Deserved to be acknowledged with sincerest gratitude is my research advisor and mentor, Dr. Robert Holz. Bob has taught me so much since I arrived at the University of Wisconsin in July 2013. Thanks for being an amazing advisor and role model in science. I am grateful also to everyone in Bob's research group, particularly Min Oo and Greg Quinn. My deepest gratitude also goes to Professor Steven A. Ackerman for seeing the potential in me to do great research. Professor Tristan L'Ecuyer and his research team have also been extremely generous with their knowledge.

Family, friends, and colleagues in the atmospheric science department have made my time as a graduate student extremely rewardable. I want to thank all of the classmates who welcomed me into this field. Thank you to all of the friends in my support system, both here in Madison and friends afar. Thank you for your love and encouragement. Lastly and most of all, thank you to my family. My parents Steve and Yolanda Ross who are the pillars of strength in my life. And my best friends, my siblings, Kat, Rebekah, and Ari. I love you all!

I have concluded through careful empirical analysis and much thought that somebody is looking out for me, keeping track of what I think about things, forgiving me when I do less than I ought, giving me strength to shoot for more than I think I am capable of. I believe they know everything that I do and think, and they still love me. And I've concluded, after careful consideration, that this person keeping score is me.

– Sam Harris

Contents

Abstract

In April 2006, the Cloud-Aerosol Lidar with Orthogonal Polarization (CALIOP) launched aboard the CALIPSO satellite and into the A-Train constellation of satellites. November 2007 marked CALIOP's change in nadir-viewing angle. The original viewing angle of 0.3° changed to 3.0°. The first and smaller viewing angle allowed the lidar to measure horizontally oriented ice crystals. Viewing ice clouds at a nadir angle closer to 0° yields specular reflection due to this oriented ice, as determined by Hu et al. in 2009. This thesis focuses on oriented ice and its correlated cloud properties. The focus is on marine midlatitude mid-low level clouds (cloud top < 5 km), where in-situ observations are difficult to achieve. The lack of consistency between cloud microphysical models and marine cloud observations motivates us to limit the subject to midlatitude regions, a region where mid-low level ice clouds are not normally thought to exist with much frequency. By collocating three instruments – CloudSat's Cloud Profiling Radar (CPR), CALIOP, and the Aqua Moderate-resolution Imaging Spectroradiometer (MODIS) – we are given a unique viewpoint into the relationships between cloud optical properties and other cloud processes such as precipitation. The lidar capabilities of CALIOP in conjunction with the microwave sensitivity to precipitation provided by the CloudSat CPR give a unique point of view to explore the connection between these two physical phenomena. Similarly, the spatial imaging from MODIS yields insights into the phase of cloud layer tops and particles' effective radii. It is found that up to 18% of warm (~ 260 K) marine mid-latitude mid-low level clouds contain horizontally oriented ice. There is also a strong positive correlation between oriented ice and surface precipitation events as detected by CloudSat. Over 70% of most oriented ice events are shown to produce surface precipitation.

List of Acronyms

CALIOP:	**C**loud-**A**erosol **Li**dar with **O**rthogonal **P**olarization
CALIPSO:	**C**loud-**A**erosol **L**idar and **I**nfrared **P**athfinder **S**atellite **O**bservations
CPR:	**C**loud **P**rofiling **R**adar
CSFOV:	**C**loudSat **F**ield **o**f **V**iew
DPR:	**D**epolarization **R**atio
FOV:	**F**ield **o**f **V**iew
HOIC:	**H**orizontally **O**riented **I**ce **C**louds/crystals. Also referred to as oriented ice crystals/clouds.
MMM:	**M**arine **M**idlatitude **M**id-low level
MODIS:	**MMMM**oderate **R**esolution **I**maging **S**pectroradiometer
NOIC:	**N**on-**O**riented **I**ce **C**louds/crystals. Also referred to as randomly oriented ice.
PIA:	**P**ath-**I**ntegrated **A**ttentuation
SST:	**S**ea **S**urface **T**emeprature
TAB:	**T**otal **A**ttenuated **B**ackscatter
V3:	**V**ersion **3** (in reference to the 2009 Version 3 CALIOP cloud phase retrieval)

Chapter 1

Introduction

Recent satellite cloud phase retrievals from Cloud-Aerosol Lidar with Orthogonal Polarization (CALIOP), a spaceborne lidar, perform with little uncertainty [6]. CALIOP detects at a vertical resolution of 30 meters. CALIOP is the most advanced long-term spaceborne lidar in the history of satellite remote sensing, providing profiles of aerosol and cloud structure. The lidar's polarization capabilities allow it to distinguish a type of cloud retrieval investigated here, named the oriented ice signature. The CALIOP Version 3 phase retrieval by Hu et al. (2009) identifies this interesting oriented signature as horizontally oriented ice crystals residing in clouds. The V3 phase retrieval can discern between oriented ice and non-oriented ice in clouds, as will be explained in Chapter 2. In marine midlatitude regions, clouds are not expected to contain ice at low altitudes. Low level ice clouds are more associated with Arctic clouds where colder temperatures exist. However, a preliminary study using the CALIOP V3 phase retrieval has shown that up to 20% of marine midlatitude mid-low level MMM cloud top retrievals are ice, and most ice is oriented ice.

This thesis is motivated by preliminary observations of horizontally oriented ice clouds which focused on oriented ice in winter 2007. Specifically, January and February of 2007. The CALIOP V3 phase retrieval partitions cloud ice into two types: oriented and non-oriented (i.e. randomly oriented). These two types of ice will hereby be referred to as **HOIC** (horizontally oriented ice clouds) and **NOIC** (non-oriented ice clouds). HOIC clouds are relatively warm compared to NOIC clouds. Clouds with NOIC peak near -33° C (240 K), while HOIC clouds peak at much warmer temperatures near -16° C (257 K) as seen in Figure 1.1. Such results and more will be explored in this research. The focus of this thesis is to more thoroughly explore oriented ice and its correlations to other cloud products using a combination of passive and active remote sensing. In this section we introduce cloud modeling and in situ observations of marine midlatitude middle to low level clouds.

Clouds require temperatures below freezing to contain ice. Supercooled liquid water droplets (water droplets with $T < 0°$ C) exist prominently between $-20° < T < 0°$ C. Mixed-phase clouds are also common and can yield ice retrievals phase retrievals at cloud top. Fully glaciated ice clouds normally exist with cloud top temperatures $T < -30°$ C. In mixed-phase clouds, precipitation is known to arise via the Bergeron-Findeisen process [20].

It is important to note that for this research, liquid water, oriented ice, and non-oriented ice do not indicate that the entire cloud is composed of that phase. Rather, that the cloud *contains* particles of that phase. The term "oriented ice clouds" may be used synonymously with "oriented ice retrievals." Oriented ice retrievals may in fact reside in a mixed phase cloud, not an ice cloud. For example, comparing HOIC to NOIC clouds simply means comparing cloud *retrievals* that are detected as NOIC or HOIC. An HOIC cloud simply contains oriented ice crystals, it is not made up

entirely of them.

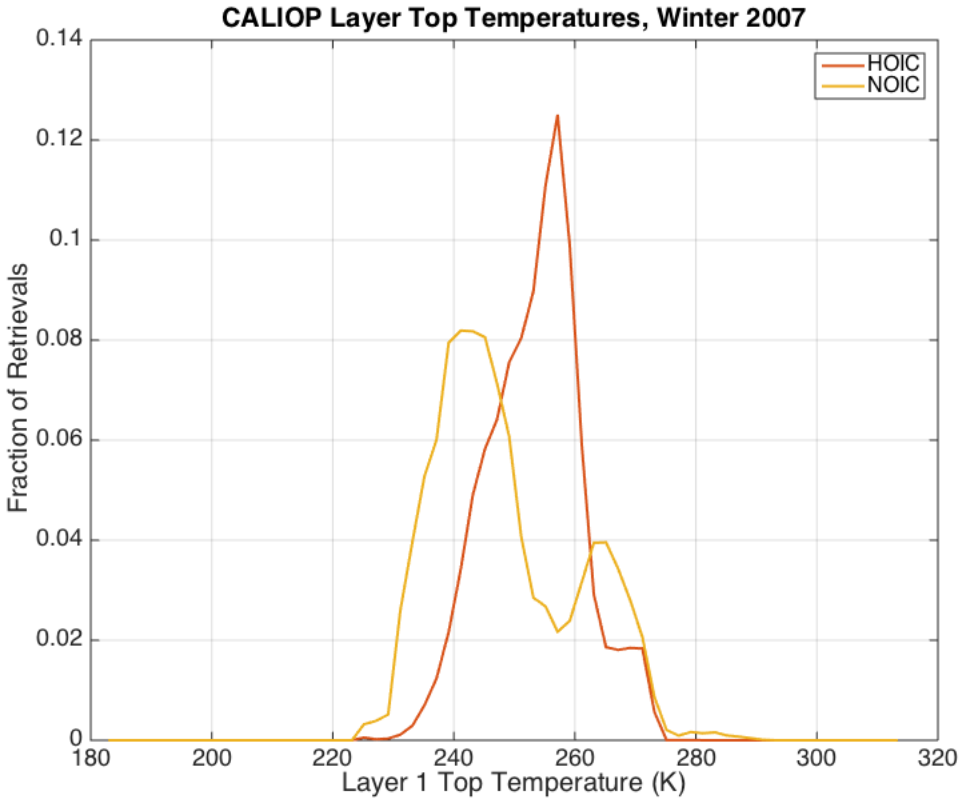

Figure 1.1: Histogram of CALIOP layer top temperatures for horizontally oriented ice (red) and non-oriented ice (orange) for January and February 2007 marine midlatitude mid-low clouds. Layer top temperatures are inferred from the layer top altitudes.

Polar-orbiting satellites provide global coverage of atmospheric properties. Having global coverage of cloud properties is useful when validating other observations such as flight campaign data, in-situ or ground-based data. However, a satellite's global perspective is especially useful in regions where there is a lack of ground-based observations, such as over oceans. While marine cloud field experiments have been conducted for quite some time, they come nowhere near observing complete ocean

coverage. Marine in-situ observations range from the tropics to the polar regions, but most observations are done in coastal regions and occur in upper or lower extremes of latitude. Hardly any field experiments are performed in marine midlatitude regions. Experiments that do overlap some midlatitudes include: the First ISCCP Regional Experiment (FIRE), the VAMOS Ocean-Cloud-Atmosphere-Land Study Regional Experiment (VOCALS-REx), and the Marine Stratus/Stratocumulus Experiments (MASE I and MASE II) [16] [25] [12]. However, these studies do not examine midlatitude marine *cloud ice* and are extremely selective in their regionality.

For an understanding of cloud ice in field experiments, it is best to turn to experiments done in Arctic regions. These include the Mixed-phase Arctic Cloud Experiment (M-PACE) and the Surface Heat Budget of the Arctic Ocean (SHEBA) [23] [27]. These field experiments are extremely useful for studying regional cloud properties, but their observations do not extend past a site-specific perspective. Little data has been collected away from coastal regions leading to a lack of measurements of cloud properties in remote marine regions, such as marine midlatitudes where extend of the ocean is vast and continental effects may vary from Arctic oceans. In order to obtain atmospheric information with full and continuous global ocean coverage, satellite remote sensing is the only viable option.

Marine stratocumulus clouds contribute significantly to defining the radiative energy budget of Earth. Clouds in general are the largest source of uncertainty in understanding Earth's radiative budget, according to the IPCC report released in 2013. This large uncertainty results from not only a lack of complete observations, but also a lack of agreement between the observations and the models [21]. Ice-containing clouds in particular are difficult to capture in cloud microphysical models.

Consistency between cloud models and observations is also an issue when it comes to precipitation. Cold and warm cloud processes treat precipitation develop-

ment differently. This research shows that a significant number of the low-altitude ice clouds in marine midlatitude environments are precipitating either mixed phase or snow at the surface (as detected by CloudSat). These and similar observations for December 2006 through November 2007 show complexities in low-level marine clouds that has not yet been observed. These observations can illuminate our understanding of relationships between cloud properties and cloud development.

Cloud microphysical models find it difficult to accurately capture the lifecycle of low-mid level ice and mixed phase clouds. Field studies such as SHEBA and M-PACE suggest that these clouds are long lived. However, traditional nucleation theories result in rapid glaciation within the cloud due to the Bergeron-Findeisen process [20]. Recent theories suggest an immersion freezing mechanism for ice nucleation, which limits the rate of formation of ice crystals within clouds [2]. This mechanism also involves a freezing point depression. De Boer et al. (2011) focus on data from three Arctic sites: two over land and one over ocean. They find that ice nucleation in stratiform clouds at these locations is likely very liquid dependent. In temperatures warmer than -20°C (257.13 K), increased ice formation occurs when there is an increased presence of liquid water.

Morrison and Pinto (2005) employ a two-moment bulk microphysics scheme in their mesoscale model to capture mixed-phased Arctic stratiform clouds [14]. They found that increasing the number of contact nuclei did not transition the mixed-phase cloud to an exclusively ice cloud, but rather just affected the partitioning between liquid and ice. The clouds monitored by Morrison and Pinto (2005) also maintained low liquid water contents, making the potential for precipitation rather low. These results are in contrast with Lohmann's (2002) cloud modeling results. Lohmann (2002) observes that increasing contact nuclei does trigger rapid glaciation, an increase in ice, and increased precipitation [11]. These and other studies exhibit

an incomplete understanding of ice cloud processes.

Cloud ice nucleation is a complex process and can occur through a variety of different mechanisms. Most studies on ice-containing clouds are all in polar regions and do not include midlatitude environments. Essentially all field experiments that aim to study lower level ice clouds are performed in Arctic regions (e.g. SHEBA, M-PACE, BASE, SEARCH). As a consequence, cloud models often turn to these Arctic field experiments for validation on ice microphysics. Clouds containing ice in mid-latitude regions are hardly explored. One of the most conclusive results that will be shown here is that cloud ice does in fact occur quite regularly. However, microphysical models do not capture the frequency and full complexity of marine midlatitude low to mid level ice clouds. Such is the motivation for this research. To improve our knowledge, this thesis focuses on marine midlatitude low clouds that contain ice. We also draw connections between these ice-containing clouds and other cloud properties such as precipitation.

Chapter 2 details the three spaceborne instruments used in this research as well as the data retrievals from each instrument. Chapter 3 describes the methodology and collocation of the three instruments, including how the dataset is compiled and how each cloud type is filtered. Chapter 4 displays major results found between cloud ice orientation and other cloud properties, highlighting precipitation results provided by the spaceborne radar CloudSat.

Chapter 2

Instrumentation and Retrievals

Beginning with the launch of Explorer 7 in 1959, satellites have monitored weather and climate on Earth. Over decades, many technological advances have been made to improve observational capabilities. In 1999, the Moderate-resolution Imaging Spectroradiometer (MODIS) launched aboard the satellite Terra as part of the NASA Earth Observing Satellites (EOS) [9]. Three years later in 2002, a twin MODIS instrument was launched aboard the Aqua satellite. In addition to collecting information on Earth's land and ocean processes, MODIS captures infrared and visible properties of clouds providing the capability to monitor global climatological cloud and aerosol properties. Being a passive instrument MODIS provides an excellent idea of spatial cloud cover and cloud properties, but lacks the ability to resolve the vertical structure of clouds and aerosols. To address the vertical dimensions, NASA developed two new observational platforms: CloudSat's Cloud Profiling Radar (CPR) and lidar CALIOP (aboard the platform CALIPSO, the Cloud-Aerosol Lidar and Infrared Pathfinder Satellite Observations). While MODIS is a passive instrument, CPR and CALIOP are active instruments. Both instruments are able

to resolve the vertical profiles of the atmosphere. CloudSat and CALIPSO were launched in April 2006 to join the A-Train. (The A-Train is a constellation of polar-orbiting spaceborne weather satellites, also called the Afternoon Consellation. MODIS, CloudSat, and CALIOP all participate on the A-Train, as seen in Figure 2.1.)

Together, CPR, CALIOP, and MODIS provide a myriad of cloud information. Each instrument operates at different wavelengths, allowing each instrument to see different information in the same cloud. MODIS's collection of wavelengths gives a unique perspective of spatial cloud optical properties. CloudSat's radar is sensitive enough to detect light precipitation and low clouds. And CALIOP's extremely high vertical resolution yields cloud and aerosol profiles with an unprecedented view. The lidar is also sensitive enough to detect tenuous clouds, unlike MODIS.

While CloudSat, CALIPSO, and MODIS fly in similar orbits, collocating the data is not a trivial task. To quantitatively inter-compare the three instruments, applying a rigorous collocation is necessary. Retrievals for each instrument are done individually with each instrument having unique spatial characteristics. In this chapter, each of the instrument's retrieval algorithms is described as well as their limitation and uncertainties. Chapter 3 will focus on the collocation process.

2.1 MODIS

MODIS is a passive sensor with a swath width of 2330 km, providing global spatial coverage every two days [9]. MODIS has 36 spectral channels between 0.415 and 14.235 μm with varying resolutions. This spectral information provides the capability to retrieve land, ocean and atmosphere properties including but not limited to cloud mask, aerosols, cloud top, cloud microphysics (e.g. optical thickness, effective

radius), cloud thermodynamic phase, and surface temperature.

Summarizing Table 1 from Platnick et al. (2003), the MODIS cloud mask (MYD35) products use as many as 20 bands, including both the visible and the infrared regions of the electromagnetic spectrum [19]. Cloud top properties (e.g. cloud top temperature and pressure) rely on the 11 μm band and bands near the 15 μm CO2 absorption region (bands 31-36). Cloud microphysical properties such as particle effective radius also rely on a wide collection of MODIS bands in the visible and infrared regions (bands 1, 2, 5, 6, 7, 20). Lastly, the MODIS cloud phase depends on the 8.5 and 11 μm bands (bands 29 and 31) for thermodynamic retrievals. In this research, we focus on the visible cloud phase retrieval.

There are some obvious drawbacks when it comes to comparing passive sensors like MODIS to active sensors like CPR and CALIOP. Because MODIS is a spatial imager, fields of view are sensitive to the mean reflectance for an entire column of the atmosphere. There will always be uncertainties in the vertical dimension of clouds. MODIS also lacks sensitivity to optically thin clouds such as cirrus. All MODIS cloud microphysical and optical property retrievals are done using look up tables (LUTs), which contain pre-calculated values of cloud properties based on the assumption of plane-parallel homogeneous clouds overlying a black surface. Separate LUTs exist for different ice habits, but most MODIS cloud retrievals are done assuming ice particles are either rosettes or aggregates [19]. Over ocean, the ice habit information is taken from the FIRE project (see Introduction and [16]), which is very regionally limited.

The collocation process, described in Chapter 3, includes MODIS products from four file types at two spatial scales: 1 km and 10 km. MODIS geolocation (MYD03), cloud mask (MYD35), and cloud products (MYD06) are at a resolution of 1 km. MODIS aerosol products (MYD04) are at a scale of 10 km. All data are from the

latest MODIS products, Collection 6.

2.2 CloudSat

The Cloud Profiling Radar (CPR) aboard CloudSat operates at 94 GHz in the microwave band (W-Band), with an along-track resolution of 1.7 km and a cross track resolution of 1.4 km, approximately. CPR profile data have 125 vertical bins, each bin with a vertical resolution of 250 m. Because CPR does not spatially scan like MODIS, it provides global coverage every 16 days. This is also the period for CALIOP's orbit.

Radars operate by sending out pulses of radiation. If these pulses hit atmospheric targets, they can echo back to be received by the radar. The determining factor in how much of the pulse gets echoed back is the cross section of the atmospheric target that the radar strikes. More specifically, the return power is dependent on the backscatter cross-section of the target. Thus, reflectivity is not a direct measurement of the mass or amount of targets in the atmosphere, but it is a quantity related to areal cross sections of atmospheric particles in a given volume. In the context of cloud profiling, radar reflectivity gives information on hydrometeors in the atmosphere. A hydrometeor is any atmospheric object that contains water, such as a rain or cloud droplet. Reflectivity is essentially a function of the amount and size of hydrometeors in the radar's sampling volume. CloudSat's minimum threshold is approximately -28 dBZ, meaning that the instrument is sensitive enough to detect very small hydrometeors.

The value that radars measure is the radar reflectivity Z. It is defined by the

reflectivity factor z as follows:

$$z = \int_0^\infty n(D)\ D^6\ dD$$

$$Z\ [\mathrm{dB}Z]\ = 10\ \log_{10}(z),$$

where z is the radar reflectivity factor, D is the droplet diameter and $n(D)$ is a size distribution function. Z is the radar reflectivity [17]. The standard units of z are $\mathrm{mm}^6/\mathrm{m}^3$, whereas the units for Z are dBZ. In the specific context of CloudSat's CPR, an equivalent reflectivity factor Z_e is actually measured. The targets in CPR's beam volume are not always spherical water droplets, but the above equations operate assuming spherical radar targets. Thus, CPR's measured Z_e may or may not be equivalent to the true reflectivity Z [17]. Further details on the Cloud Profiling Radar and its reflectivity retrievals can be found in Tanelli et al. (2008) [22].

Radar reflectivity is not a direct measurement of the mass of water in the atmosphere. Radar reflectivity is more akin to a measurement of drop size distribution in a given volume; the determining factors of Z are the size of the hydrometeors and the number of hydrometeors in a volume. In the case of precipitation, a radar reflectivity signal is dominated by falling hydrometeors (i.e. precipitation). Z generally increases as precipitation becomes larger in size. Some qualitative and approximate thresholds for ground based weather radars are: $Z \approx 5$ dBZ is very light mist, $Z \approx 20$ dBZ is light rain, $Z \approx 35$ is moderate rain, and $Z \approx 50$ is heavy rain.

Relating reflectivity measurements to direct measurements of precipitation (i.e. rain rates in [mm h^{-1}]) is a complex task. The National Weather Service has defined multiple Z-R Relationships, or relationships relating the reflectivity, Z, to

an estimated rain rate, R. However, these relationships are extremely region specific. To relate global precipitation measurements to rainfall rates, the CloudSat precipitation retrieval requires a complex algorithm.

This research highlights precipitation products provided by the Cloud Profiling Radar. CloudSat precipitation algorithms can determine whether or not precipitation is occurring, what the phase of the precipitation is (e.g. rain or snow), and at what intensity it is precipitating. Because CPR is an attenuating radar, standard precipitation algorithms can lead to a false estimation of rainfall rates when they exceed 1.5 mm h^{-1}. The CloudSat precipitation algorithm developed by L'Ecuyer and Stephens (2002) applies the two-way path integrated attenuation (PIA) to correct for attenuation [10]. The PIA estimates the total attenuation through the column. The PIA, measured attenuated radar reflectivity, and known surface properties are all required to estimate the unattenuated radar reflectivity profile. The surface information becomes somewhat simplified when limited to marine scenes. Over oceans, CloudSat algorithm uses the sea surface temperature (SST) and wind speed to gauge the ocean surface roughness, as it determines how the radar signal is echoed to the receiver and measured. CloudSat precipitation retrievals are only performed for the column when precipitation is detected at the surface (four bins above the surface bin). Detecting reflectivity directly at the surface can cause problems. A radar signal that echoes off of a ground surface can cause what is referred to as ground clutter. Near the surface, the radar signal becomes too noisy to resolve the lower 1-3 bins. Thus, when CloudSat gives surface quantities, they are taken from four bins above the surface bin.

The collocation in this research uses five CloudSat files as input. All CloudSat products have the same spatial resolution of roughly 2 km. The geolocation is taken from the Level 1B CPR files. The Level 2B GEOPROF files give all the basic

reflectivity information and cloud masks. Level 2C files include all of the advanced precipitation information. The 2C-PRECIP-COLUMN files contribute precipitation incidence and phase, as well as the path-integrated attenuation and other variables involved in the precipitation algorithm. The 2C-RAIN-PROFILE and 2C-SNOW-PROFILE files give precipitation intensity for rain and snow, respectively.

2.3 CALIOP

The Cloud-Aerosol Lidar and Infrared Pathfinder Satellite Observations (CALIPSO) platform is home to a lidar named CALIOP (pronounced like *Calliope*). The lidar operates at two wavelengths, 532 nm (visible) and 1064 nm (near-infrared) with the 532 nm channel having polarization capabilities. CALIOP has a high vertical resolution of 30 m, which makes it perfect for detailed profiles of clouds and aerosols. CALIOP products are distributed with three varieties of horizontal resolution: 1/3 km, 1 km, and 5 km. For this research, only the CALIOP Level 2 Layer products are investigated, having resolution of 5 km spatially. CALIOP can distinguish up to 10 unique vertical layers in any atmosphere and provides properties for each of those layers.

A lidar determines the distance to a remote target by illuminating it with a pulsed laser. CALIOP can determine the return power at any range r from the lidar. Because CALIOP looks downward from space, it collects curtains of vertical data of the atmosphere. From Pirronen (1994), the lidar equation can be defined as:

$$P(r) = E_0 \, \frac{cA}{2\pi r^2} \left[\frac{3}{8\pi} \beta_m(r) + \frac{\rho(\pi, r)}{4\pi} \beta_a(r) \right] e^{-2 \int_0^r \beta_e(r') dr'} + M(r) + b,$$

where P is the incident lidar power returned to the receiver, r is the range, c is the speed of light. A is the area of the receiver, $\beta_a(r)$ is the aerosol scattering cross-section per unit volume, $\beta_m(r)$ is the molecular scattering cross-section, and $\beta_e(r)$ is the extinction cross-section per unit volume. Finally, $\rho(\pi, r)$ is the aerosol backscatter phase function, $M(r)$ is the multiply-scattered return, and b is the background signal [18].

The lidar gathers the range and properties of a target by analyzing the reflected laser signal. Relevant to understanding this research are two CALIOP data products, the Total Attenuated Backscatter (TAB) and the Depolarization Ratio (DPR). TAB, γ, for a cloud layer is defined as the sum of the perpendicularly polarized component of the total backscatter signal, $I_\perp$ and the parallel-polarized component, $I_\parallel$, as follows:

$$\gamma = I_\perp + I_\parallel.$$

It is essentially a measurement of the calibrated intensity of the backscattered lidar signal as a function of range [8]. The depolarization ratio, δ, is defined as the ratio of these two polarization components:

$$\delta = \frac{I_\perp}{I_\parallel}.$$

DPR is a measurement of how much the lidar target is depolarizing the signal, or changing its polarization. If a target is smooth and uniform and the signal hits the surface of the target at an incident angle, the signal will not become depolarized. If the target is more irregular and has a rougher surface, the signal becomes depolarized. The non-smooth microphysics of more irregular particles treats the perpendicular and parallel components of the light differently, resulting in a change

from the original polarization.

The collocation in this research requires only two CALIOP file types, both with an along-track resolution of 5 km. (The collocation described in the next chapter uses the 1 km geolocation to find collocation indices, but applies them to these 5 km products.) These are the Cloud Layer (CAL-CLAY) files and the Aerosol Layer (CAL-ALAY) files.

2.4 CALIOP Level 2 data

CALIOP is capable of providing profiles of the atmosphere for every point in its orbit. However, for the purpose of collocation, only the CALIOP Level 2 Layer products are included in this research. In addition to providing a high resolution profile for every point, the CALIOP data algorithm can also define up to 10 distinct layers of any field of view.

The CALIOP Layer identification algorithm essentially consists of two steps. First, distinct layers are identified by a set of algorithms that are collectively known as the Selective Iterative Boundary Locator [24]. These algorithms are applied to the profiles from the 532 nm channels. A layer is defined when the received signal is from a purely molecular signal (i.e. when there are neither clouds nor aerosols in an atmospheric column). Next, a second set of algorithms classifies these boundaries into type: either cloud or aerosol. Using all three channels (two 532 nm channels and one 1064 nm channel), the cloud type (e.g. liquid water or ice) and aerosol type (e.g. coarse or fine). As Winker et al. (2009) states, "If multiple cloud and/or aerosol layers are found in a column, scene classification and extinction retrieval are performed on the uppermost layer first. Classification and retrieval then proceed downward, layer by layer, so that scene classification of lower layers can be based

on signals corrected for the attenuation of the overlying layers" [24].

This thesis emphasizes the CALIOP Version 3 phase retrieval, detailed in the next section. Additional products included in this research stem from feature altitudes. For example, once CALIOP has defined the altitudes of the top, base, and therefore middle of a cloud, CALIOP algorithms can infer the temperature and pressure at the cloud top, cloud base, and cloud midlayer.

2.5 CALIOP Version 3 Phase

The polarization capabilities of the 532 nm channels on CALIOP allow the instrument to detect cloud phase with fairly high confidence. In 2009, Hu et al. released the newest version of the CALIOP cloud phase retrieval (Version 3, or V3). In V3, Hu et al. examine the relationship between depolarization and backscatter for cloud particles [6]. This new phase discrimination allows CALIOP to distinguish not only between liquid water particles and ice particles in clouds, but also discriminate between certain types of ice, namely horizontally oriented ice crystals and randomly oriented ice crystals.

Prior to the V3 phase retrieval, the CALIOP phase retrieval was performed under the assumption that a backscattered signal from ice crystals is depolarized, whereas the signal from liquid water droplets is not depolarized due to the spherical nature of the drop. However, Hu et al. (2009) demonstrate that because of CALIOP's field of view, the instrument can measure significant depolarization in the presence of liquid water drops due to multiple scattering. In addition to depolarizing water droplets, there can also exist a subset of non-depolarizing ice crystals. Ice crystals that do not depolarize are said to be horizontally oriented, exhibiting specular reflection that does not depolarize the lidar signal. The traditional view of strongly depolarizing

ice crystals is still true for randomly oriented ice crystals. The irregular orientation of these ice crystals strongly depolarizes the lidar signal.

Specular reflection is most associated with mirror-like reflection. The physical mechanism that characterizes specular reflection is that radiation from a singular incident direction will be reflected in a singular outgoing direction. This contrasts with diffuse reflection, where the outgoing radiation can be reflected in multiple directions with multi-component polarization due to the irregularity of the target. The depolarization in the case of ice crystals occurs due to the multiple inter-reflections occurring within the target. Thinking in the context of polarization, the polarization of the incoming light does not change during specular reflection. The outgoing radiation will have the same polarization as the incoming radiation when reflected off of a smooth surface. The return powers for the lidar when observing HOIC versus NOIC are very distinguished, as seen in Figure 2.2(a).

When CALIPSO was first launched in 2006, the lidar had a viewing angle of 0.3°, very near nadir. This low angle resulted in the first signals of CALIOP to have very intense backscatter for a significant fraction of cirrus measurements with the specular return from oriented ice crystals dominating the CALIOP return signal in many scenes. To reduce the contribution from horizontally oriented ice crystals, the CALIOP viewing angle was tilted to 3°. This allows for more accurate retrievals of cloud phase and vertical extinction profiles [6]. Consequently, CALIOP's ability to detect the specular signal was reduced drastically. This effect can be seen in Figure 2.2(a) where there are three regimes of cloud phase defined by Hu et al. (2009). The left panel includes retrievals in October 2007, when CALIOP's viewing angle was 0.3°. The right panel includes retrievals from November 2007, when the viewing angle was changed to 3°. Retrievals with low depolarization and high attenuated backscatter are considered to be horizontally oriented ice crystals (HOIC). Retrievals

with high depolarization and low attenuated backscatter are considered to be non-oriented ice crystals (NOIC). The middle regime, with moderate depolarization and moderate backscatter is composed of liquid water retrievals. Liquid water is shown to experience surprising amounts of multiple scattering, which results in the moderately depolarized return signal. This figure also shows that once the viewing angle was increased to 3°, the retrievals of HOIC are eliminated.

Due to the nature of specular reflection, we can infer that oriented ice retrievals are due to flattened ice particles, namely plates or columns [26]. These are the only known ice habits that would cause a specular return signal. Other ice habits, such as bullet rosettes and needles, would not exhibit specular reflection and would be detected by the CALIOP phase retrieval as non-oriented ice, depolarizing at much higher values.

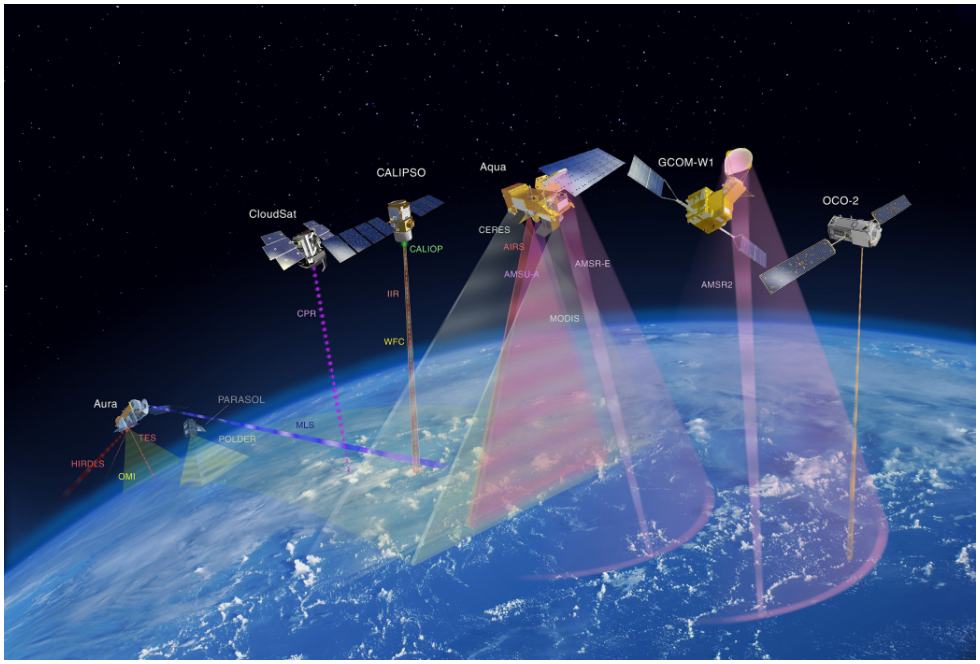

Figure 2.1: The Afternoon Train (A-Train) constellation of satellites. Photo courtesy: NASA.

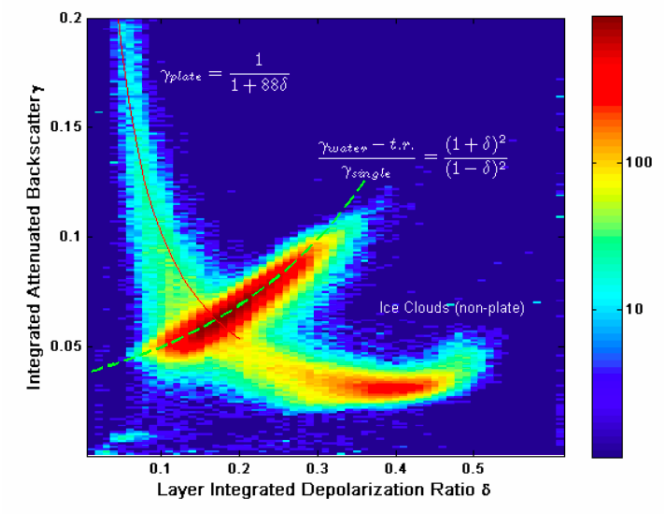

(a) Viewing angle of 0.3°.

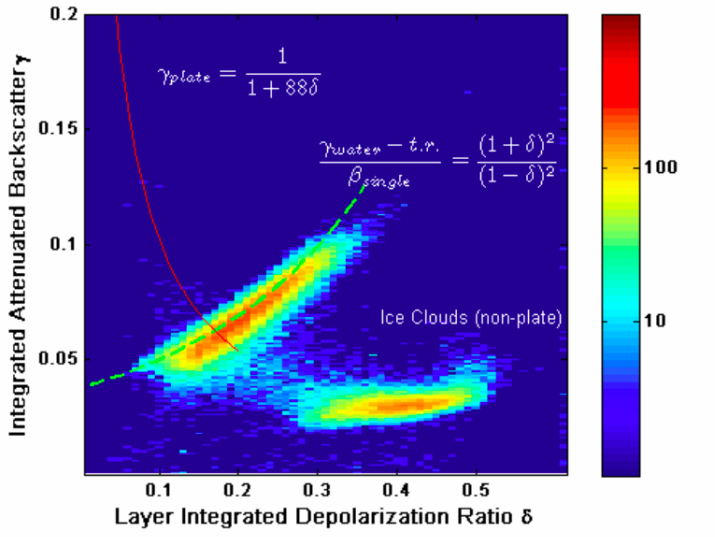

(b) Viewing angle of 3°.

Figure 2.2: The depolarization – attenuated backscatter relation for two CALIOP viewing angles. Three cloud phase types are shown: oriented ice, liquid water, and non-oriented ice. High backscatter γ and low depolarization δ correspond to oriented ice. Low backscatter γ and high depolarization δ corresponds to non-oriented ice. Moderate backscatter and depolarization corresponds to liquid water clouds. CALIPSO lidar measurements during the 0.3° viewing angle period and (b) during the 3.0° viewing angle period. The oriented signature vanishes once the viewing angle changes to 3.0°. Image courtesy Hu et al. (2007) [5].

Chapter 3

Collocation Methodology

3.1 Collocation overview

The collocation method in this research involves spatially matching data from three satellite instruments: MODIS, CloudSat (CPR), and CALIOP. The fields of view of these instruments vary widely. CloudSat has the largest field of view (FOV) out of all three instruments; the FOV is approximately 2 km^2. Whereas MODIS MYD03 geolocation has a resolution of 1 km for every field of view and CALIOP Level 1 geolocation has a resolution of 330 m.

The collocation process at pixel level includes three major steps. First, mapping multiple 1 km^2 MODIS images to a single 2 km^2 CPR image. Then, mapping multiple 20 $\times$ 330 m CALIOP images to the same 2 km^2 CPR image. Lastly, data from both pixels are combined. The result is one pixel whose spatial scale is 2 km^2. This process is done for multiple variables (i.e. *data products*) from the instruments. The result is a collection of points, divided into a set granule size. Fill values are used when appropriate. A schematic of this process at a pixel level can be seen in

Figure 3.1.

When the sizes of the required input files from each satellite are considered, the process becomes slightly more complicated. The Level 1 files from the three instruments each cover different spatial domains, as seen in Figure 3.2(a). One CloudSat granule contains approximately 1:40 hours worth of orbit. This is equivalent to 37,000 CPR points, each point consisting of a 2 km^2 thick curtain of the atmosphere. Geographically, one CloudSat granule spans from equator to equator as the blue line in Figure 3.2(a). One CALIOP granule spans roughly 50 minutes of orbit, depicted by the red line in Figure 3.2(a). Each granule contains anywhere from 55,000 to 65,000 points. Each point is roughly 20 $\times$ 330 m spatially and contains a curtain of information, similar to CloudSat. Compared to the CPR, however, CALIOP has much higher vertical resolution. Lastly, each MODIS granule spans 5 minutes of orbit as seen in the green area in Figure 3.2(a). MODIS images are approximately 2030 pixels $\times$ 1354 pixels, each pixel being 1 km^2 spatially.

Collocation indices are found by supplying Level 1 Hierarchical Data Format (HDF) files to software provided by Dr. Fred Nagle at the Space Science and Engineering Center. Collocation between MODIS-CloudSat and CALIOP-CloudSat are done individually. (For example, the MODIS-CloudSat matchup results in indices that when applied, yield Figure 3.2(b). The CALIOP-CloudSat collocation results in indices applied to the files in Figure 3.2(a) would yield a portion of the orbit that CALIOP and CloudSat have in common; in this case it is the entire CALIOP orbit since the CALIOP granule's domain is embedded spatially within the CloudSat granule.) To combine MODIS, CloudSat, and CALIOP, the CALIOP-CloudSat collocated products are truncated to match with the shorter MODIS-CloudSat portion of the orbit. The result of the entire process is a single HDF file including MODIS, CloudSat, and CALIOP products. The along-track index across each instrument is

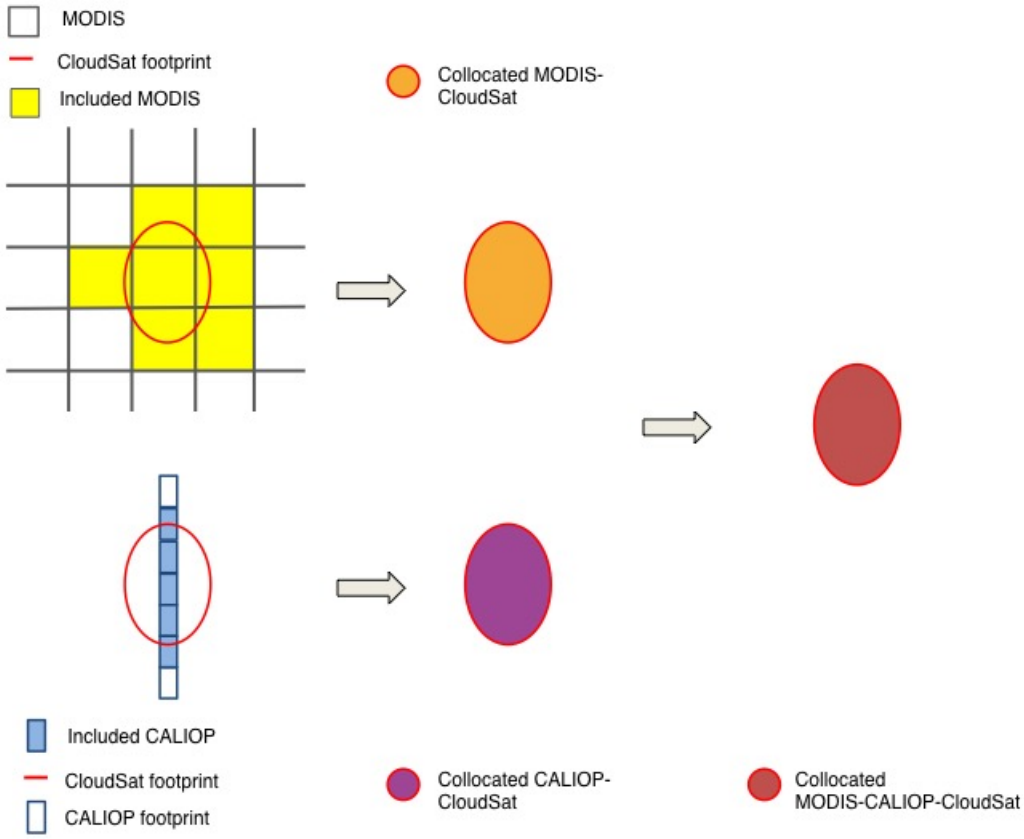

Figure 3.1: Schematic flow chart of the collocation process on a pixel level. Collocation between MODIS-CloudSat and between CALIOP-CloudSat are done individually, then combined to result in a FOV that contains data from all instruments, but now at the same resolution.

the same, averaging roughly 1,800 points for non-edge cases, such as the example in Figure 3.2.

3.2 Data averaging

This section details the data products from each satellite that are included in the collocation process. Attention must be given to how the data are handled and averaged to fit a CloudSat FOV. A significant challenge is preserving the vertical information offered by CloudSat and CALIOP. For one-year worth of A-Train orbit, saving every profile for every field of view would require a large amount storage space and would be difficult to process. The collocation code in this research strategically applies averaging, layering, and integrating to the CloudSat and CALIOP data. This section will describe these techniques in detail. The MODIS averaging is also discussed.

3.2.1 CloudSat

In the collocation, CloudSat is considered to be the master field of view; i.e. we are mapping the other observation onto the CloudSat's FOV (CSFOV) as explained in the previous section. Therefore spatial averaging of the CloudSat data products is not required. Averaging is applied to the data vertically. Saving 125 vertical bins for each point for 12 months would require far too much space, especially since we plan to collocate with two other instruments.

To keep the output files a reasonable size, the vertical resolutions in both CloudSat and CALIOP are compressed. Rather than saving the high-resolution reflectivity profiles from CPR, data can be averaged, divided into layers, column-integrated, or filtered selectively to reduce the space required to save data for every point and make

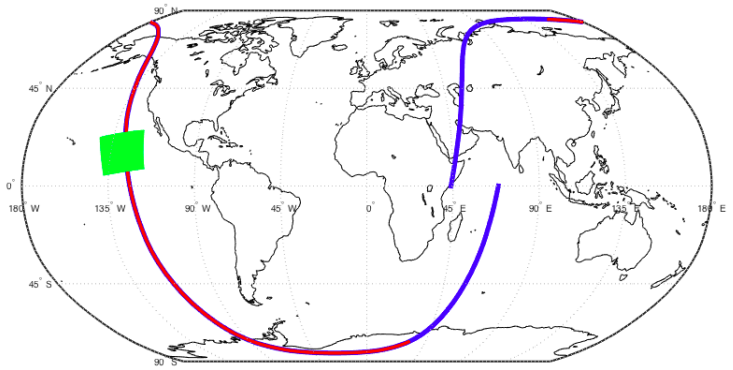

(a) Input granule sizes

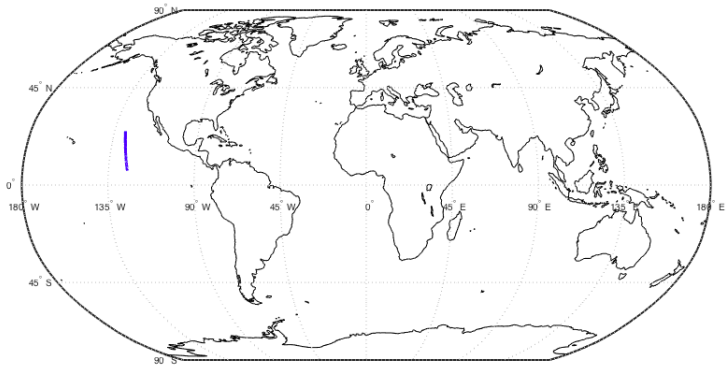

(b) Output granule size

Figure 3.2: (a) Sizes of individual CloudSat (blue), CALIOP (red), and MODIS (green) granules. (b) Size of the output granule containing data from all three instruments. The output granule spans the locations where all three instruments from (a) overlap.

the match files easier to filter and analyze. For this reason most of the CloudSat data products that are included in the final output collocation file are one dimensional. The two dimensional CloudSat products that preserve vertical information are all from CloudSat precipitation files (i.e. PRECIP-COLUMN, RAIN-PROFILE, SNOW-PROFILE). The original profiles provided in the Level 2C data are divided into five levels, where the CloudSat bins define the level boundaries. The original 125 vertical CloudSat bins are grouped into groups of 25 bins, hence the consequent five level structure. The altitudes (or range heights in CloudSat terminology) at which each level top and level base reside are also saved in the output file. The products that this vertical filtering is applied to are the snow rate and its uncertainty, the liquid water content, the ice water content, the snow water content and its uncertainty, the snow Log N_0 and its uncertainty, and the snow Log Lambda and its uncertainty.

Most CloudSat data included in the output files are original data from CloudSat files that has simply been spatially selected and included in the output file. Some CloudSat profiles are chosen to be appropriate for this data. For example, the maximum above-ground reflectivity and height at which this maximum reflectivity occurs is saved for each point. From the CloudSat Cloud Mask profile, the cloud top height is saved. This cloud top height is the maximum height of the top range bin where the cloud mask is certain (CloudSat Cloudmask = 40). Three column-integrated CloudSat products are included as well. These are the liquid water path, ice water path, and snow water path.

3.2.2 MODIS

All MODIS data, unlike CloudSat data, are taken spatially and do not have a second vertical dimension. For every CloudSat FOV (CSFOV), there can be up to seven MODIS pixels that fit within that CSFOV. Collocation indices provided by software developed by Dr. Fred Nagle identify which (up to) seven MODIS pixels fit within a certain CSFOV [15]. The data from those seven pixels are then averaged and this averaged value is assigned to the single CSFOV. This process repeats for every CloudSat point.

The main challenge that arises when mapping MODIS data to the CloudSat FOV is how to handle the quality assurance (QA) data products. Imagine having seven MODIS pixels that will be mapped onto one CloudSat pixel, as in Fig 3.1. Each of the seven MODIS pixels have their own uncertainty, or QA flag. Averaging seven different uncertainty values and assigning that value to one pixel does not accurately preserve the quality assurance information. For example, if within our seven original MODIS pixels, four are retrieved with an uncertainty of 10%, and three are retrieved with an uncertainty of 80%. This averages to a total uncertainty of 40%, not capturing the high quality of the data whose uncertainty were only 10%.

The matchup software has been developed to preserve the quality of the MODIS data. It involves applying QA flags and uncertainties to the data prior to applying the collocation and averaging. One way to think of this is making multiple aggregates of the MODIS data. The aggregates are slightly different, ranging in the selectivity of the data quality. The collocation indices are then applied to each version. For example, take MODIS optical thickness (OT), which is given by the MYD06 optical properties file. Before applying the collocation indices and averaging, four versions of the MODIS OT are saved. The first version is the original version with all points

included. The second version is slightly refined, where all points with an uncertainty greater than 50% are excluded from the collocation and averaging. The third version takes this a step further and excludes all points with an uncertainty greater than 20%. Lastly, the fourth version of the data is very selective and excludes all points with an uncertainty greater than 10%. This final version is considered the highest quality of data. This type of QA filtering is applied to MODIS optical thickness and effective radius.

Data provided from the MODIS aerosol files (MYD04) have a coarser resolution than the other MODIS products. Instead of a spatial scale of 1 km, MYD04 products have a resolution of 3 km. This requires simply divided the collocation indices by three. A similar type of quality filtering is applied to the MODIS aerosol optical depth (AOD) products. Instead of filtering with uncertainty values, a quality flag (QF) named the Land Ocean Quality Flag is used. This flag has three integer values 0, 1, 2, and 3. These values essentially correspond to bad data, good data, better data, and best data, respectively. The four versions of MODIS AOD filters take surface type into account. The four levels of filtration of AOD are as follows: First, the original AOD with no data removed. Second, a version where land AOD retrievals with quality flag < 2 and ocean AOD with QF < 1 are excluded. Third, the land AOD retrievals with quality flag < 3 and ocean AOD with QF < 1 are excluded. Lastly, a version where the land quality flag < 3 and ocean AOD with QF < 2 are excluded. These four versions of AOD are saved in the output as *unfiltered, good, better*, and *best.*

Returning to the MYD06 optical cloud properties, effective radius retrievals are separated into ice and liquid retrievals. The phase discrimination is determined by the MODIS visible phase retrieval (from MYD06, this is the Cloud Phase Optical Properties product), which is done entirely independently of the CALIOP V3 Phase

retrievals. From these phase retrievals, we also calculate a liquid water fraction and ice fraction for every output pixel. Returning to the example schematic in Figure 3.1, if four of the pixels are retrieved as ice and three are retrieved as liquid water, then the resulting collocated MODIS-CloudSat pixel will have an ice fraction of 4/7 or approximately 0.571 and a liquid fraction of 3/7, or approximately 0.429.

An additional modification is made to the MODIS optical thickness and effective radii retrievals. The original data products from the MYD06 files do not include cloud edges. This inclusion requires adding "partly cloudy" (PCL) points to the original data. These PCL products include data "from points identified as either partly cloudy from 250-m cloud mask test or 1-km cloud edges." Data are saved that both include and do not include these partly cloudy points. For example, for optical thickness, eight final versions of optical thickness are included in the output: four versions with varying QA and no edges included, and four QA-varying versions with edges included. Standard deviations for every product are saved, except for the aerosol data from the MYD04 files.

3.2.3 CALIOP

The CALIOP collocation indices are computed at the 330 m spatial resolution. However, we wish to apply these indices to CALIOP data that has 5 km resolution. This involves simply dividing the CALIOP indices by fifteen and rounding up to the nearest integer (330 m $\times$ 15 $\approx$ 5 km).

As aforementioned, the CALIOP data included in this process are from the CALIOP Layer products only: the Cloud Layer (CLAY) 5 km files and the Aerosol Layer (ALAY) 5 km files. The full CALIOP data profiles are not included. The averaging in the collocation process is very similar to that described for MODIS in

the section above. The main difference is that collocation indices must be applied to each CALIOP layer. CALIOP layer data have up to ten layers, where layer one is highest in altitude. An overview of the layer retrieval can be found in section 2.4. For every CALIOP layer detected in a granule, the collocation averaging is performed within that layer. Averaging is done not across layers, but rather treats each CALIOP layer individually. Up to eight spatial CALIOP pixels can fit into one CSFOV. The data from those (up to) eight pixels is averaged and assigned to one CSFOV. This process is repeated for every CALIOP layer. The result is a two dimensional CSFOV-sized pixel that contains the layer information. The first dimension of course is spatial, and the second dimension preserves the vertical layer information originally provided by CALIOP.

Again, the issue of how to treat uncertainties and quality flags arises when averaging multiple pixels to one CSFOV. However, we treat this issue differently than in the MODIS case. Instead of applying QA filters to CALIOP products before applying the collocation and averaging, the QA data are simply averaged just as the data products are. CALIOP data included in the output matched files has not been screened, while screening was applied to the MODIS observations. Actual QA values and uncertainties that have been averaged from CALIOP are included in the output collocation files. QA may be applied to the CALIOP data once the match files have been generated.

The focus of this research is determining correlations based on the CALIOP V3 Phase Retrieval (see section 2.4). Like MODIS, CALIOP retrieves the phase of the cloud. However, instead of dividing cloud phase simply into liquid water and ice, CALIOP provides further information about the type of ice. CALIOP can distinguish cloud pixels as having one of three distinct phases: liquid water, horizontally oriented ice, and non-oriented ice. Once the collocation averaging is

applied to the CALIOP cloud phase, each resulting FOV contains a liquid fraction and ice fraction. For any FOV where the ice fraction is nonzero, the resulting FOV contains an oriented fraction. This oriented fractions says when there is ice, what fraction of that ice is oriented. Even if the resulting FOV has an ice fraction of 0.2, if all of that ice oriented, then the oriented fraction of the FOV is 1.0. Any FOV whose ice fraction is 0 (i.e. there is no ice in that pixel) has an oriented fraction of a fill value.

3.3 Processing

The NASA Atmosphere Science Investigator-led Processing Systems (SIPS) is the means by which all output files are created. We will refer to these output collocation as "match" files. Greg Quinn, a team member of SIPS, processed the software that describes the collocation methods in previous sections of this chapter. Performing such a task for one year of data requires the following to produce each output file: First, collocation indices are found with the aforementioned software from Fred Nagle (see [15]). This is done to the Level 1 geolocation files for each instrument, CloudSat, MODIS, and CALIOP. The indices are then and applied to all which is sometimes at different resolutions than the indices are given. spanning 12 months of A-Train orbit. The output files span December 1, 2006 to November 17, 2007.

3.4 Cloud filtering

This research focuses on **m**arine **m**idlatitude **m**id-to-low level (MMM) clouds. To confine the data to include only this subset of clouds, a combination of data from all three instruments is used. The geolocation filtering uses CloudSat coordinates; our

midlatitude cases are filtered to contain only retrievals where the CloudSat latitude is between 30° and 60° N or S. To include only marine cases, the MODIS land-sea mask is implemented. All fields of view where the MODIS land-sea mask ≥ 6 are considered to be marine cases. Lastly, we include only clouds where the CALIOP Layer 1 Top Altitude is less than 5 km. In other words, we are considering only cases where there are no higher clouds. The highest cloud top must reside at an altitude less than 5 km. The purpose of this is to rule out any cirrus cases. We wish to compare only lower clouds to one another.

The clouds and their phases are determined using only the CALIOP Layer 1 data. Layers below layer 1 are not considered in this work unless otherwise stated. Clouds are filtered into three exclusive regimes: liquid water, oriented ice, and non-oriented ice. Points that contain both liquid water and ice are excluded. Points that contain both oriented ice and non-oriented ice are also excluded. However, the amount of fields of view that are mixed in phase or mixed in orientation is small. Neglecting points where the cloud contains multiple phases or multiple orientations does not significantly diminish the dataset. As seen in Figure 3.3, most of the CALIOP retrievals in February 2007 when averaged to fit the CSFOV are either exclusively cloudy or exclusively not cloudy. These statistics are including all clouds in February 2007, not limiting to the MMM subset. It is apparent that there are few retrievals (2.08% of retrievals) where the cloud fraction is between 1 and 0. Similarly, there are few retrievals (1.56%) where the ice fraction (and liquid fraction) is between 1 and 0. Even within ice orientation, there are few retrievals (4.42%) where the oriented fraction is between 1 and 0 (Figure 3.3). This justifies excluding retrievals with values between 0 and 1. As mentioned in the introduction, this does not mean that all clouds in the MMM subset are either exclusively liquid or ice. Many of the clouds are actually mixed in phase, but at a pixel level, each retrieval is likely either

exclusively one cloud phase.

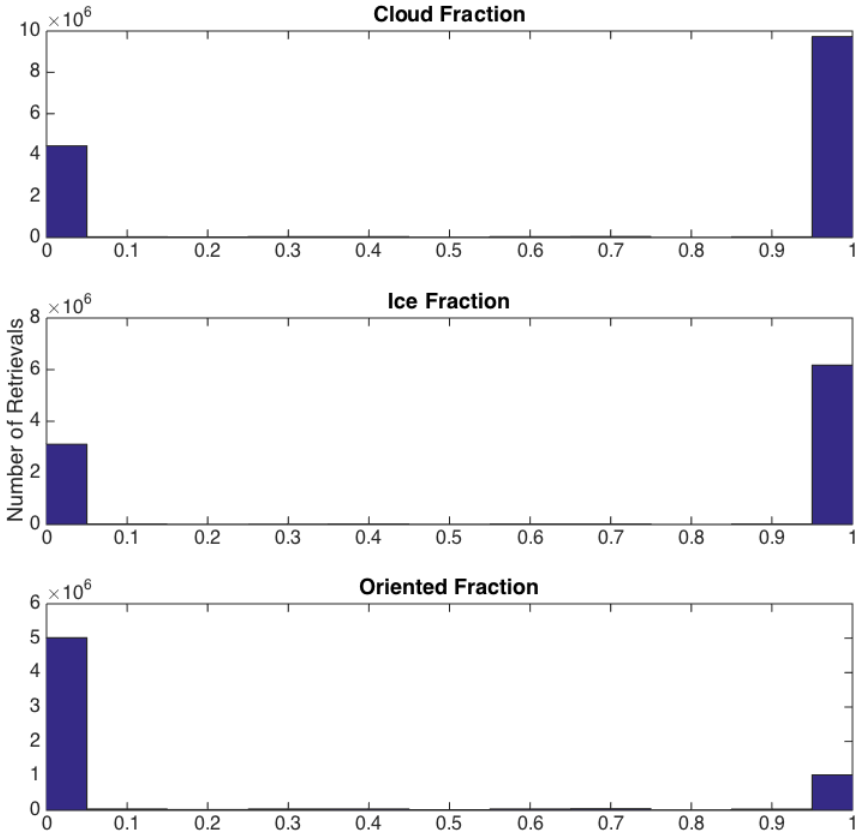

Figure 3.3: Histogram of Cloud Fraction, Ice Fraction, and Oriented Fraction for all clouds in CALIOP Layer 1 for February 2007. Retrieval counts are not limited to MMM clouds; rather, include land and ocean, all latitudes, and all cloud heights in the CALIOP Cloud Layer 1 files. The values for these three variables are almost exclusively 0 or 1.

Chapter 4

Results

This chapter explores the correlations between CALIOP cloud phase and collocated cloud data from CloudSat and MODIS. We begin with a case study of oriented ice and precipitation in the North Pacific ocean, then view oriented ice on a global scale for a twelve month timescale.

The total collocated data spans twelve months: December 2006 through November 2007. All results in this section include only CALIOP cloud retrievals that fit within the category of **m**arine **m**idlatitude **m**iddle to low altitude clouds (MMM) unless stated otherwise. To reiterate from the previous section, this subcategory is defined by cloud cases that fit the following criteria:

Marine: Location with a land/sea flag ≥ 6 (from MODIS).

Midlatitude: Location must be between 30° and 60° N or S (from CloudSat).

Mid-low level: Cloud Top Height < 5 km (from CALIOP).

Some results in this section divide marine midlatitude regions into five marine subregions: North Pacific, North Atlantic, South Pacific, South Atlantic, and South Indian oceans. These subregions can be seen in Figure 4.1.

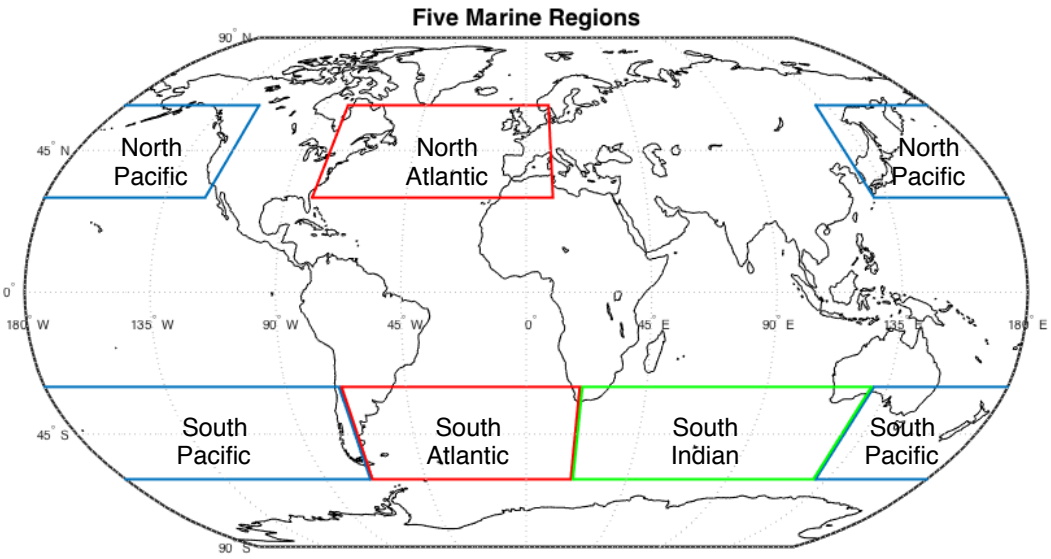

Figure 4.1: Map of the five marine regions: North Pacific, North Atlantic, South Pacific, South Atlantic, and South Indian Oceans.

First, we examine a case study of oriented ice from 2007 in the Northern Pacific in Section 4.1. Section 4.2 details the incidence of oriented ice in marine midlatitude mid-low clouds. Section 4.3 compares bulk cloud properties of HOIC versus NOIC. Next, we compare CALIOP cloud phase to MODIS cloud phase in section 4.4. Section 4.5 contains all results pertaining to CALIOP cloud phase and CloudSat precipitation variables, including precipitation incidence, phase, and intensity.

4.1 A case study: February 21, 2007, 21:30Z in the North Pacific

Northern cold months are when oriented ice is most likely to be found, as will be discussed in later sections. The case study shown in Figures 4.2 and 4.3 is in the Northeast Pacific on February 21, 2007 at 21:30Z. Figure 4.2 shows spatial MODIS data of the scene in which our case resides. The CALIOP and CloudSat orbit spans 43° N to 45° N, as highlighted in red in Figure 4.2. Figure 4.3 has five panels: three panels of CALIOP data and two panels of CloudSat data. The top three panels display from top to bottom: CALIOP Layer 1 Cloud phase and ice orientation, CALIOP Total attenuated backscatter, and CALIOP depolarization ratio, respectively. The fourth panel is CloudSat's radar reflectivity in dBz, followed by the CloudSat surface precipitation flag in the fifth panel, which tells whether or not CloudSat detects precipitation at the surface.

There is a copious amount of open-cell convection in this area off of the western coast of North America, seen in the left panel of Figure 4.2. The unique oriented signature explained in Chapter 2 with the $\delta - \gamma$ relationships can be seen very clearly in the first three panels of Figure 4.3. Note that the latitude range highlighted by

the red box shows high attenuated backscatter, low depolarization, and does indeed correspond to a phase retrieval of oriented ice. This same cloud feature corresponds very well to surface precipitation as detected by CloudSat. The radar reflectivity exceeds values of 15 dBz. Further, the CloudSat precipitation flag also detects certain precipitation.

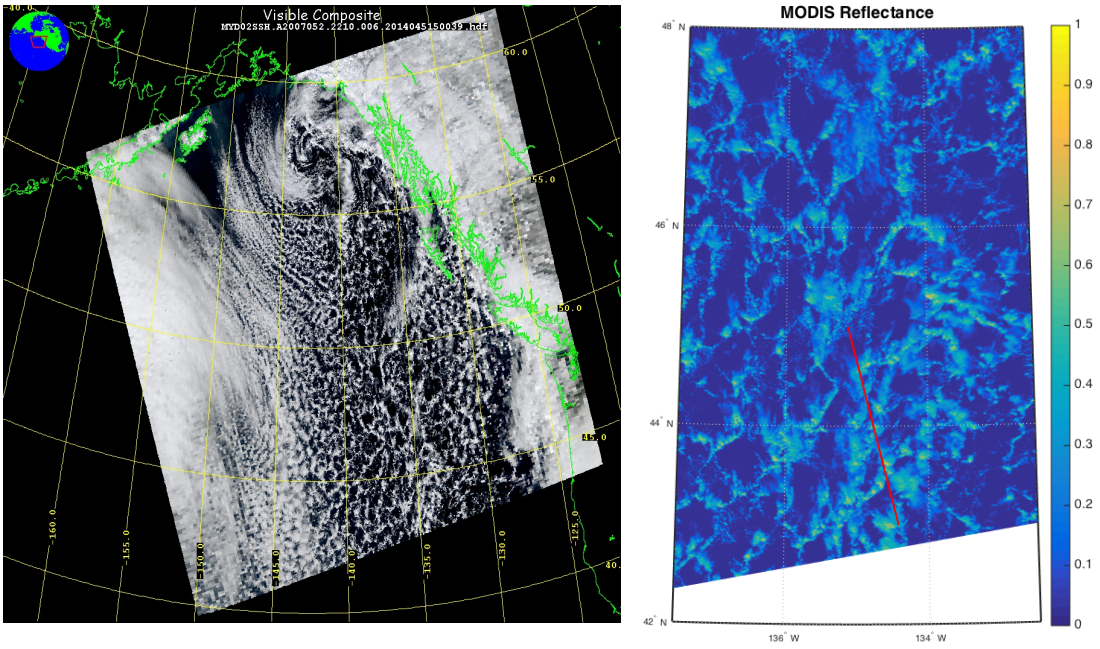

Figure 4.2: MODIS reflectance of the scene of the case study above the North Pacific for February 21, 2007 at 21:30:55 UTC. The panels are (left) zoomed out true color MODIS reflectance of the case study and (right) a closeup view of the MODIS visible reflectance. The CALIOP and CloudSat orbit is the focus of our case study and the path is highlighted in red. True color panel on the left is courtesy of NASA LADS.

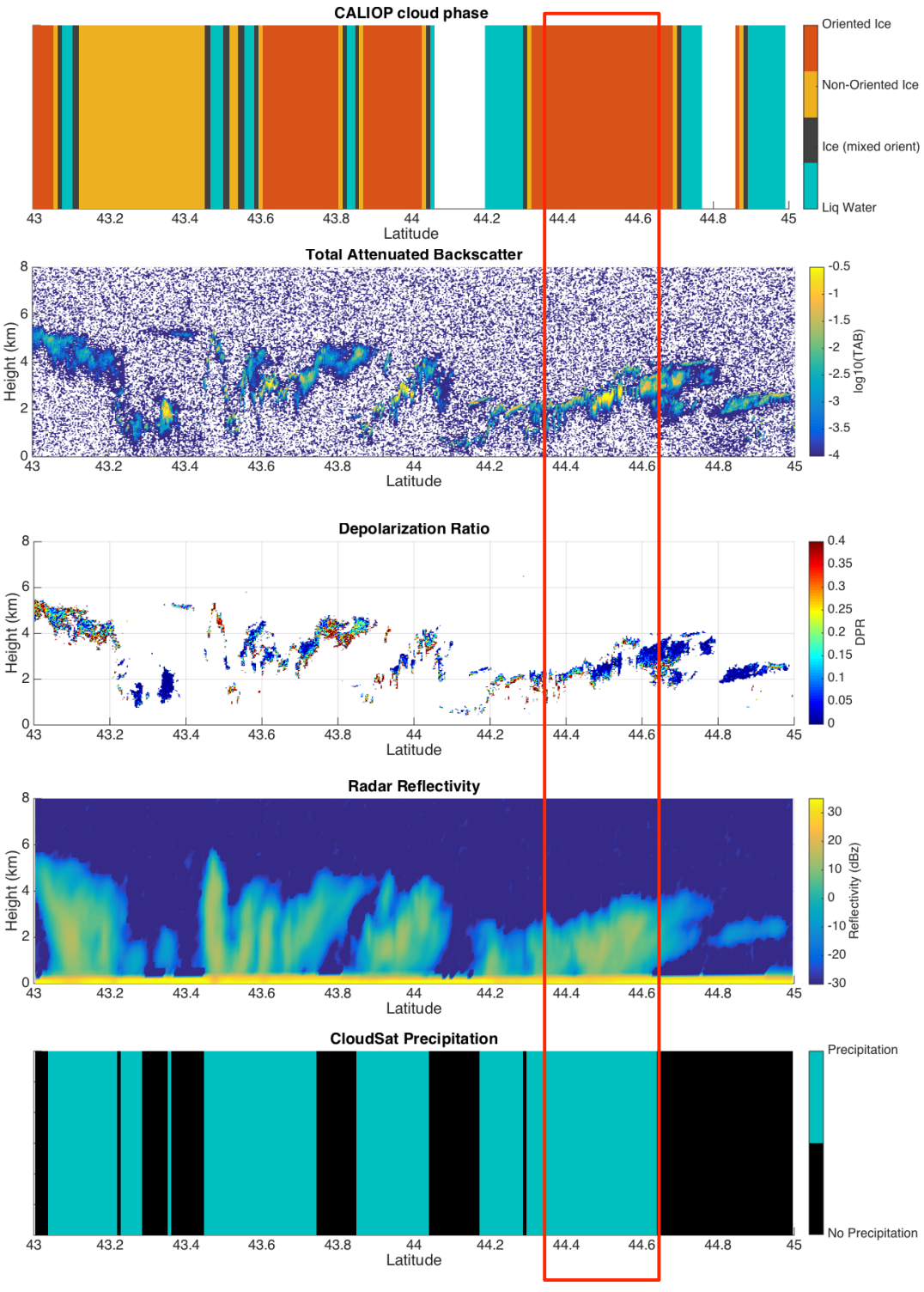

Figure 4.3: A case study above the North Pacific for February 21, 2007 at 21:30:55 UTC, data shown span 43° N to 45° N. Panels from top to bottom are: CALIOP cloud phase type for Layer 1, CALIOP profile of total attenuated backscatter γ, CALIOP profile of depolarization ratio δ, CloudSat profile of radar reflectivity Z, and the CloudSat surface precipitation incidence flag. Areas of oriented ice (high backscatter and low depolarization) tend to correspond with surface precipitation as detected by CloudSat.

4.2 Regionality and seasonality of oriented ice

This section investigates the regions and seasons where oriented ice is most likely to occur. We investigate what fraction of marine midlatitude mid-low level (MMM) clouds contain total ice, and partition ice into oriented and non-oriented ice (i.e. Total cloud ice is composed of two exclusive types: oriented and non-oriented.) The fraction of clouds that are liquid is simply one minus the total ice fraction. Three fraction values are shown in Figures 4.4 through 4.6: the oriented ice fraction, non-oriented ice fraction, and total ice fraction. Each figure shows a different region. Figure 4.4 contains only marine midlatitude mid-low clouds in the northern hemisphere, between 30° N and 60° N. Figure 4.5 contains only MMM clouds in the southern hemisphere, between 30° S and 60° S. Figure 4.6 focuses on MMM clouds in the northern pacific, between 30° N and 60° N in latitude and between 130° E and 120° W.

There is more annual variation in the northern hemisphere (NH), where the ice fraction peaks at 0.18 in February and is generally high for December through April. The NH ice fraction drops below 0.05 in June, July, August, and September. In the southern hemisphere (SH) winter, the ice fraction hits a maximum of 0.075 in July, much lower than the northern hemisphere maximum. The SH ice fraction is less than 0.05 for more than half of the observed months: December, January, February, March, April, October, and November.

Focusing on the North Pacific, the seasonal variation in MMM ice cloud occurrence is even more prominent. The fraction of HOIC cases with respect to all cloud cases reaches a maximum of 0.18 in April. This high incidence of oriented ice clouds in marine midlatitude mid-low cases is high even for months with moderate temperatures. High amounts of HOIC in the NP continue from December 2006 until June

2007 as seen in Figure 4.6.

Gridded monthly concentrations of oriented ice events for marine midlatitudes are shown in Figure 4.7. Seasonal groups of three months are averaged to find the total count of each $3^\circ \times 3^\circ$ grid. Months are grouped into winter (December 2006 through February 2007), spring (March through May 2007), summer (June through August 2007), and autumn (September through November 2007). For example, in the winter months of December, January, and February, the monthly concentration of HOIC events off the coast of Siberia exceed 200 counts per month. Across DJF, MAM, JJA, and SON, the color scales in these figures are identical. These plots include only counts from marine midlatitude mid-low oriented ice cases.

The most prominent pattern consists of high concentrations of HOIC in the Northern Pacific cold months. Density values exceed 250 per grid box for nearly half of the year, from December through May. The high HOIC values in the Northeast Pacific appear lagged and do not become prominent until February. Northern summer sees a dramatic drop in HOIC events. Similarly, Southern summers are sparse, but cover large spatial scales beginning in May in the South Atlantic. Southern cold months do not experience the high concentrations that are seen in Northern winter and spring. These gridded densities indicate that the Southern oceans experiences less variation in HOIC events than the Northern oceans. There are also huge marine midlatitude areas that contain no HOIC retrievals.

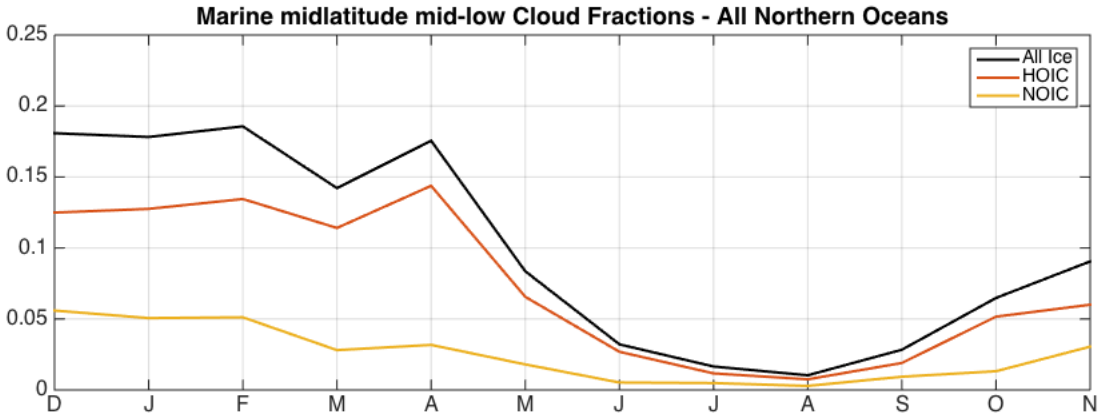

Figure 4.4: Ice cloud fractions for the Northern Hemisphere MMM cases; for each of the twelve months. Total ice fractions (black), oriented ice (red), and non-oriented ice (orange) are shown. The sum of HOIC and NOIC equals the number of total ice retrievals.

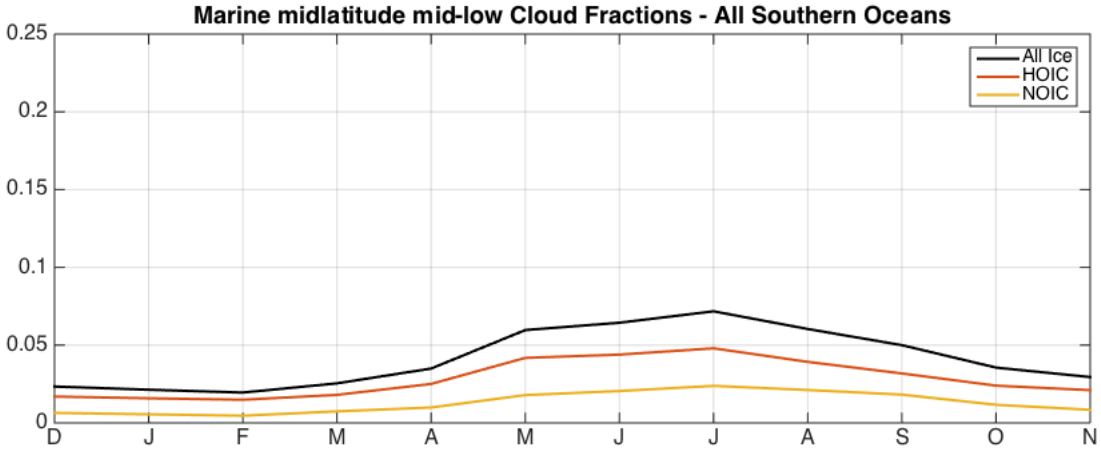

Figure 4.5: The fractions of all MMM clouds that are ice (black), HOIC (red), and NOIC (orange). Cases are limited to the Southern Hemisphere.

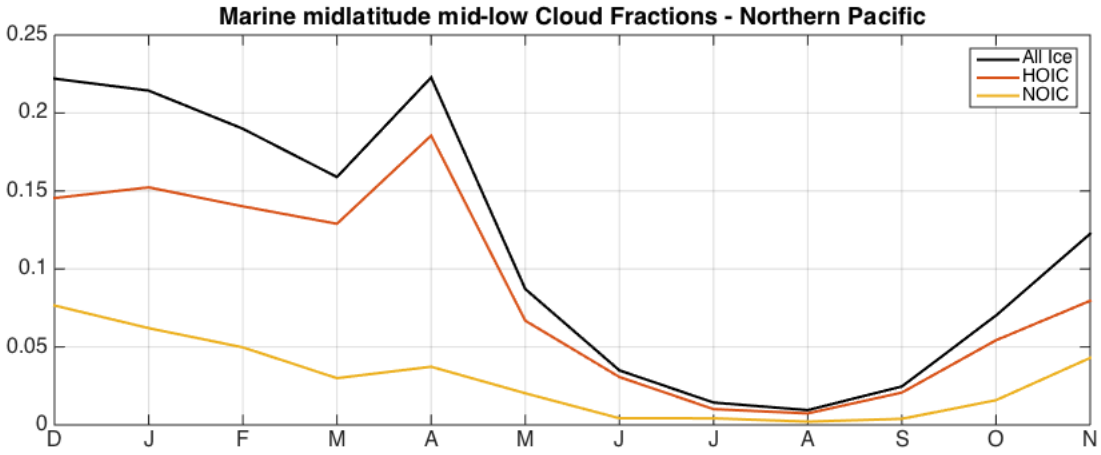

Figure 4.6: The fractions of all MMM clouds that are ice (black), HOIC (red), and NOIC (orange). Cases are limited to the Northern Pacific marine region.

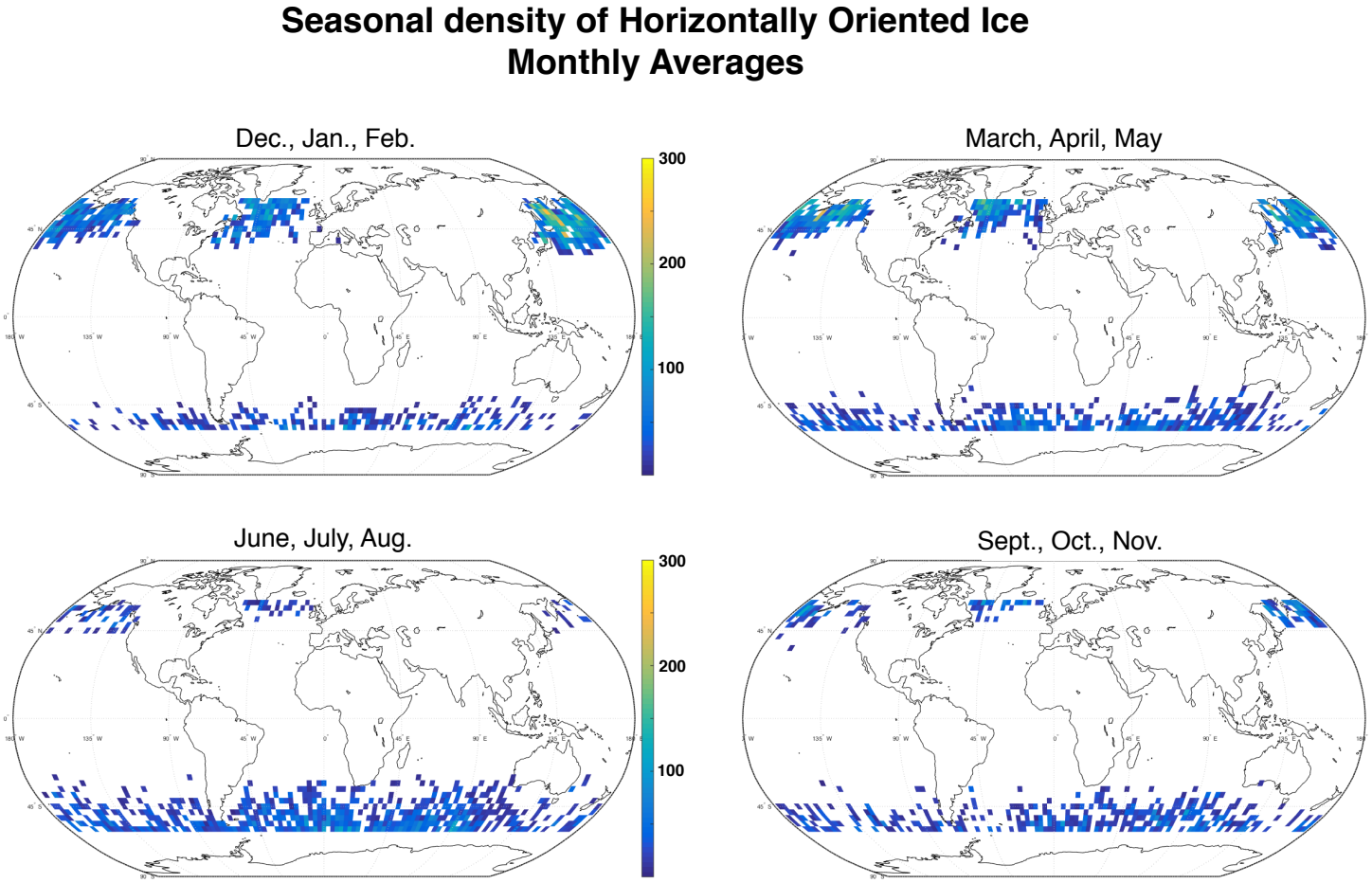

Figure 4.7: Density of horizontally oriented ice retrievals for four seasons. Clockwise from the upper left: winter DJF, spring MAM, summer JJA, and autumn SON. Densities are gridded to 3° grids. Counts from each set of three are normalized by three, so the quantities may be considered as monthly averages representing seasonal time scales.The color scale on all plots is identical. Values of the color scale can be seen next to the DJF and JJA panels.

4.3 Ice orientation and cloud properties from MODIS and CALIOP

Figures 4.8(a), 4.8(b), and 4.9 show normalized histograms of CALIOP layer top altitude, CALIOP layer top temperatures, and MODIS effective radii, respectively. All histograms compare oriented ice to non-oriented ice, where the phase discrimination is applied using the CALIOP V3 Phase Retrieval. A normalized histogram, instead of showing the total number of counts for every bin, normalizes by the total count of cloud type. A normalized histogram shows the fraction of retrievals that fit within a bin.

Note that MODIS can only retrieve effective radius values during daytime, as it is a passive sensor and uses solar reflectance methods. Thus, only very small fractions of HOIC and NOIC have valid effective radius retrievals. In addition, there are some cloud retrievals where CALIOP detects ice but MODIS detects liquid. This will be seen in the next section, and is another contributor to low effective radius retrievals in CALIOP ice pixels.

Figure 4.8(a) reveals that most NOIC marine midlatitude mid-low clouds reside at the higher extreme of our 0-5 km range. HOIC have a higher chance of existing at lower altitudes, many with cloud top heights less than 3 km. Other differences between oriented ice and non-oriented ice are seen in Figure 4.8(b). The temperature histogram for NOIC retrievals appears bimodal, with most retrievals corresponding to cloud top temperature near -33° C (∼240 K). Temperatures for HOIC exist in a smaller range of temperatures, and most retrievals are warmer, at -16° C (∼257 K). This temperature is only slightly below freezing and is considered fairly warm for ice clouds. It is likely that HOIC is being retrieved at the top of a mixed phase cloud that contains oriented ice.

Correlations between ice orientation and MODIS effective radii show a noticeable trend. Figure 4.9 shows oriented ice (red) having slightly larger effective radii than NOIC (orange). Most marine midlatitude mid-low HOIC have ice effective radius retrievals near $r_{\text{ef}} = 45$ μm. NOIC tend to correspond to smaller effective radii, most MODIS retrievals near $r_{\text{ef}} = 32$ μm.

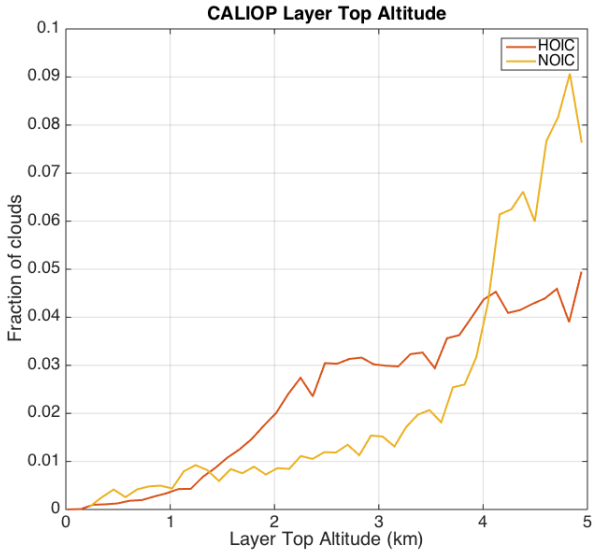

(a) Altitudes of layer 1 top. HOIC vs NOIC.

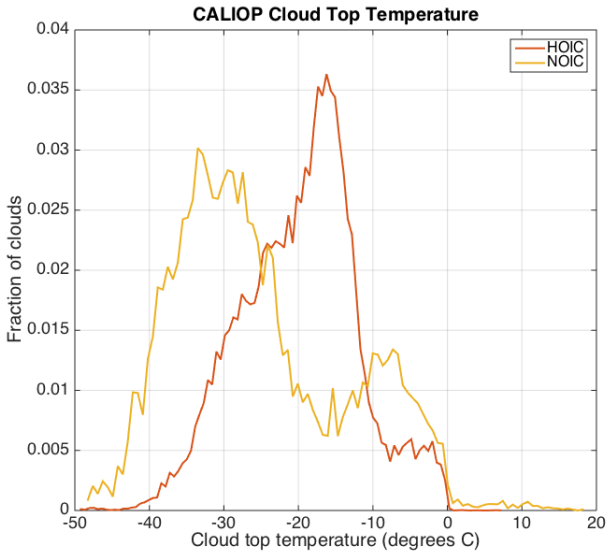

(b) Temperatures of layer 1 top. HOIC vs NOIC.

Figure 4.8: Cloud heights and temperatures: marine midlatitude mid-low ice clouds for twelve months, December 2006 - November 2007. (a) Normalized histogram of CALIOP layer top altitudes for oriented ice (red) and non-oriented ice (orange). Only clouds that fit into the MMM cloud subset are included. (b) Normalized histogram of CALIOP layer top altitudes for oriented ice (red) and non-oriented ice (orange). Only clouds in the MMM cloud subset are included in these bin counts.

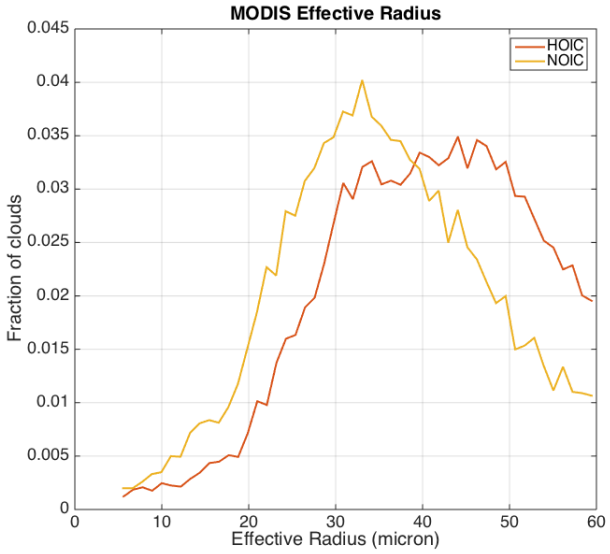

Figure 4.9: Effective radius for marine midlatitude mid-low ice clouds for twelve months, December 2006 - November 2007. Normalized histogram of MODIS ice effective radii for oriented ice (red) and non-oriented ice (orange). Only cases that are retrieved by both MODIS and CALIOP as ice are included in these statistics.

4.4 CALIOP cloud phase and MODIS visible cloud phase retrievals

Here, the MODIS visible cloud phase retrieval is compared to the CALIOP cloud phase retrieval. Cases are included only when the CALIOP Layer 1 cloud top altitude is less than 5 km. This ensures that MODIS is observing low clouds as well. Cases are also limited to include only when CALIOP detects ice in all cloud layers. In cases where CALIOP detects ice above liquid in a cloud, the footprint is not included. Here we examine three categories of ice clouds. First, where all CALIOP Layers are exclusively ice that can be mixed in orientation. Second, where all CALIOP Layers are exclusively horizontally oriented ice. Lastly, where CALIOP layers are exclusively non-oriented ice.

Figure 4.10 shows the fractions of all marine midlatitude mid-low ice that correspond to MODIS zero and nonzero ice fraction values. Over 85% of CALIOP ice-only cases are detected by MODIS as having no ice within the field of view. (Recall that these footprints are the size of a CloudSat field of view. CALIOP-MODIS collocation is not performed at resolutions smaller than a CloudSat footprint, despite both CALIOP and MODIS having smaller spatial fields of view.)

Also shown in Figure 4.10 are MODIS ice fractions but for oriented versus non-oriented ice retrievals. For each type of ice orientation, only points are included where CALIOP detects either exclusively oriented ice or exclusively non-oriented ice in *all* layers; points where the layer ice is mixed in orientation are not included. Over 70% of NOIC correspond to no ice from the MODIS retrievals. 65% of oriented ice fields of view contain no ice from the MODIS retrievals. There are apparently stark differences between the cloud phase retrievals of CALIOP and MODIS's visible channels. There is poor correlation between the ice phase retrievals of these two

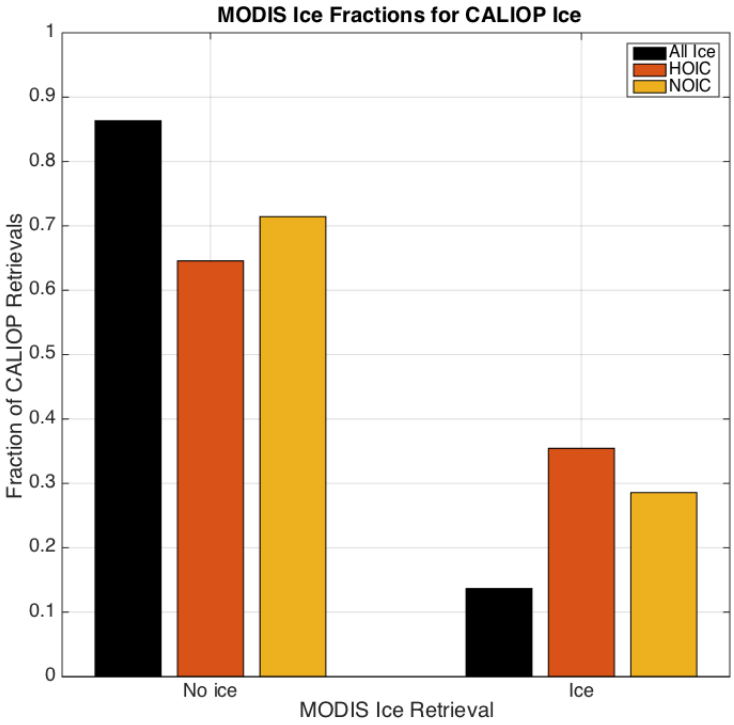

Figure 4.10: Normalized histogram of MODIS ice fraction when CALIOP detects exclusively ice in all layers of a pixel. All counts include marine mid-latitude lower cloud cases from December 2006 through November 2007. In black, counts include exclusive ice layers but may be mixed in ice orientation. In red are cases where all layers are oriented ice. Orange bars include cases where all layers are non-oriented ice.

instruments once mapped to a footprint equivalent to CloudSat's field of view.

4.5 CloudSat precipitation

The results in this section focus on the collocation between CALIOP cloud phase and CloudSat precipitation data with the goal of investigating the relationship between ice habit (NOIC and HOIC) and precipitation. This includes both precipitation phase (i.e. rain or snow) and correlations with precipitation intensity.

4.5.1 Ice orientation and precipitation incidence

This section details the tendency for cloud phases to experience surface precipitation. Surface precipitation is given by the CloudSat precipitation flag data product. The precipitation fraction for liquid, oriented ice, and non-oriented ice clouds is defined by:

$$\text{Precip. } \textit{cloud phase} \text{ fraction} = \frac{\text{number of precipitating } \textit{cloud phase} \text{ retrievals}}{\text{number of total } \textit{cloud phase} \text{ retrievals}},$$

Where the *cloud phase* is either liquid, oriented ice, or non-oriented ice in the MMM cloud subset. And precipitating cases include both rain and snow, certain and possible cases defined by the CloudSat Precipitation Flag product. The criteria for rain, snow, and mixed classifications are as follows:

Precip Flag = 1, 2, 3	Rain
Precip Flag = 4, 5	Snow
Precip Flag = 6, 7	Mixed Phase.

The precipitation fraction is normalized by the total number of clouds of that phase; not the total number of precipitating cases. Out of all MMM precipitation, the precipitation fraction does not tell you the likelihood of the cloud phase from which precipitation is sourced. Rather, it says that when a certain cloud phase is occurring, what the likelihood is that the cloud precipitates. Recall that usually 80% or more of marine midlatitude mid-low clouds are liquid water. Thus, when precipitation occurs, it is most likely to be coming from liquid clouds since these are the most populous. The precipitation fractions in this section, rather, tell you the tendency for a certain cloud phase to be precipitating.

The most apparent result from Figure 4.11 is that the HOIC (red line) has consistently higher precipitation fractions than the liquid (blue line) and NOIC (orange line) cloud retrievals. DJF North Pacific and North Atlantic oriented ice clouds have precipitation fraction of 0.78, 0.74, 0.7 in the NP ocean and 0.78, 0.75, 0.74 in the NA ocean. In the southern ocean regions, HOIC precipitation fraction values often exceed 0.7 as well in winter months. With non-oriented and liquid cloud cases, precipitation values never consistently reach values as high as in HOIC cases as demonstrated in Figure 4.12, where bulk cases of all marine midlatitude mid-low clouds of each phase are counted. Out of the total oriented-ice cloud cases, 78% are precipitating, whereas only 47% of NOIC and 29% of liquid water clouds correspond to surface precipitation. There is a strong positive correlation between oriented ice and surface precipitation.

4.5.2 Ice orientation and precipitation phase

The topic now shifts from precipitation incidence to precipitation phase. Instead of all precipitation, cases are split exclusively into rain, snow, and mixed precipita-

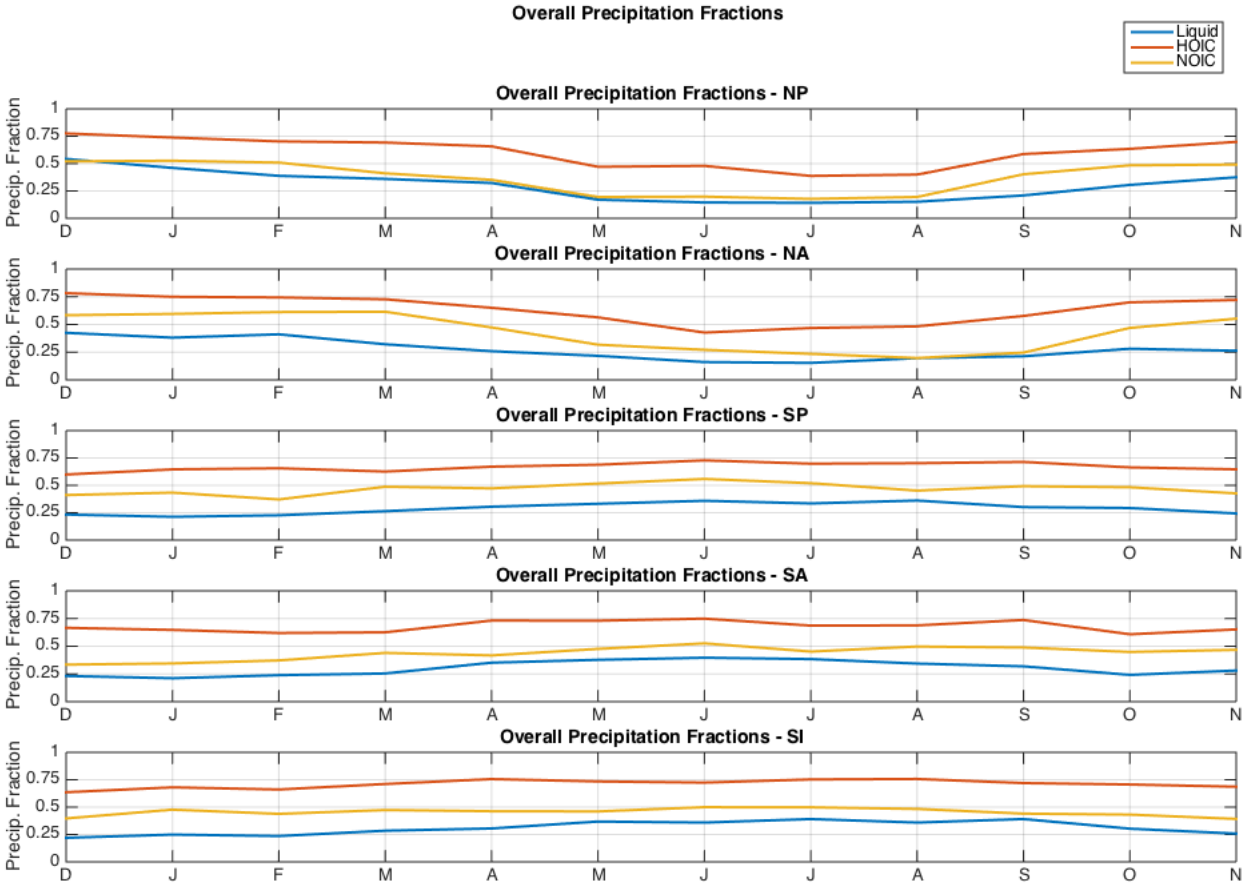

Figure 4.11: Precipitation fractions of liquid, oriented ice, and non-oriented ice clouds from December 2006 through November 2007. Each of the five marine regions is shown, from the top down: Northern Pacific, Northern Atlantic, Southern Pacific, Southern Atlantic, and Southern Indian oceans. Liquid water fractions are in blue, horizontally-oriented ice fractions are in red, and non-oriented ice fractions are in orange.

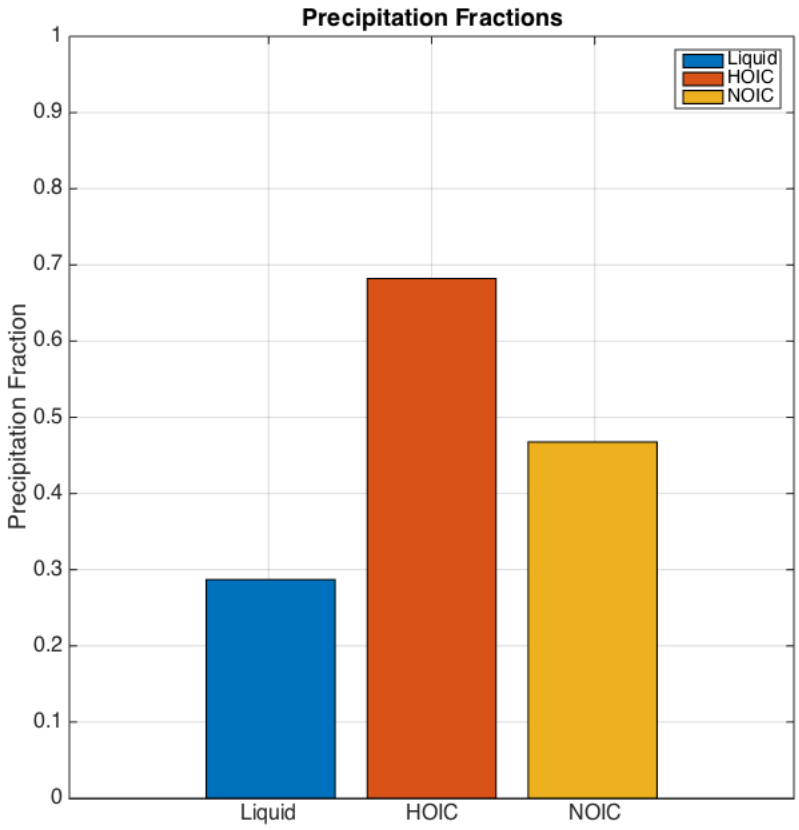

Figure 4.12: Bulk precipitation fractions of liquid, oriented ice, and non-oriented ice clouds. Counts combine all marine regions and all twelve months. Liquid water fraction is blue, horizontally-oriented ice fraction is red, and non-oriented ice fraction is orange.

tion phases. The mixed precipitation phases are defined according to temperature thresholds in the CloudSat precipitation algorithm. Precipitation phase is classified at the CloudSat surface (i.e. four bins above the surface bin). Hence, we are focusing on surface precipitation only. The results in this subsection focus on the correlations between the three surface precipitation phase types – rain, snow and mixed – and the cloud phase types – liquid, oriented ice, and non-oriented ice. The precipitation phase is determined by the product *CloudSat Precipitation Flag* in the 2C-PRECIP-COLUMN files. Flag values of 1, 2, or 3 are *rain*, 4 or 5 are *snow*, and 6 or 7 are *mixed phase precipitation*. There are three types of precipitation phase fraction, i.e. rain fraction, snow fraction, and mixed fraction. Each cloud phase type has three corresponding precipitation phases that give the likelihood that that cloud is precipitation a certain phase.

For example, the **rain fraction** for liquid, oriented ice, or non-oriented ice clouds is defined as:

$$\text{Rain fraction} = \frac{\text{number of raining } \textit{cloud phase} \text{ retrievals}}{\text{number of total precipitating } \textit{cloud phase} \text{ retrievals}},$$

And the **snow fraction** for a cloud type is:

$$\text{Snow fraction} = \frac{\text{number of raining } \textit{cloud phase} \text{ retrievals}}{\text{number of total precipitating } \textit{cloud phase} \text{ retrievals}},$$

Where again the *cloud phase* is either liquid, oriented ice, or non oriented ice cloud retrievals. In both cases, rain and snow fraction are normalized by the total number of precipitating clouds of that phase. Such that for a given month and region, the

sum of the counts of rain retrievals, snow retrievals, and mixed phase retrievals equal the total number of precipitating retrievals.

Each of the figures below show data from a single cloud phase. Within each figure, the three precipitation phases are examined. Figures either show precipitation phase fractions for each month and region, or they show bulk precipitation phase fractions for all months and all regions. Again, these quantities are only within a certain cloud phase.

Figures 4.13 and 4.14 show liquid cloud precipitation phase fractions. The figures show sequenced/regional and bulk precipitation phase fractions, respectively. Most summer liquid clouds, when they are precipitating, are raining. This is true in the North Pacific, North Atlantic, and South Pacific regions, but the relation is less existent in the Southern Atlantic and Indian oceans. The winter NP, SA and SI regions experience nearly equal amounts of mixed phase precipitation, snow, and rain. In the bulk counts of liquid clouds, over 50% are raining. Precipitating liquid clouds are over 30% mixed in phase and 17% snow.

Figures 4.15 and 4.16 show precipitation phase fractions for oriented ice clouds. Again, most northern summer HOIC clouds are raining. For summers in the southern hemisphere, however, HOIC clouds are more likely to experience mixed phase precipitation. Winter months in both northern and southern oceans are most likely to precipitate either snow or mixed phase, with a higher tendency for mixed in NP, NA, and SP regions. The tendency for HOIC to precipitate mixed phase is reiterated in the bulk counts, seen in Figure 4.16. Almost half of all HOIC clouds precipitate mixed, where roughly 25% precipitate snow and rain, with a slight favor of the former.

The tendency to produce rain in summer months is again seen in Figure 4.17 for non-oriented ice clouds. In the monthly and regional plots in Figure 4.17, there

is a strong relationship between raining cases and NOIC clouds for the NP, NA, and SP summer cases. Winter cases in the NP, NA, and SA regions have a strong chance of snow. Such high snow fractions are not seen for any other cloud phases. Winter NOIC mixed precipitation fractions nearly reach 50% in some cases, as well. Examining the bulk counts of NOIC clouds (Figure 4.18), there is a slight overall favor for non-oriented clouds to precipitate snow. The order of preference then follows as snow, then rain. So, both oriented and non-oriented clouds are least likely to be precipitating rain.

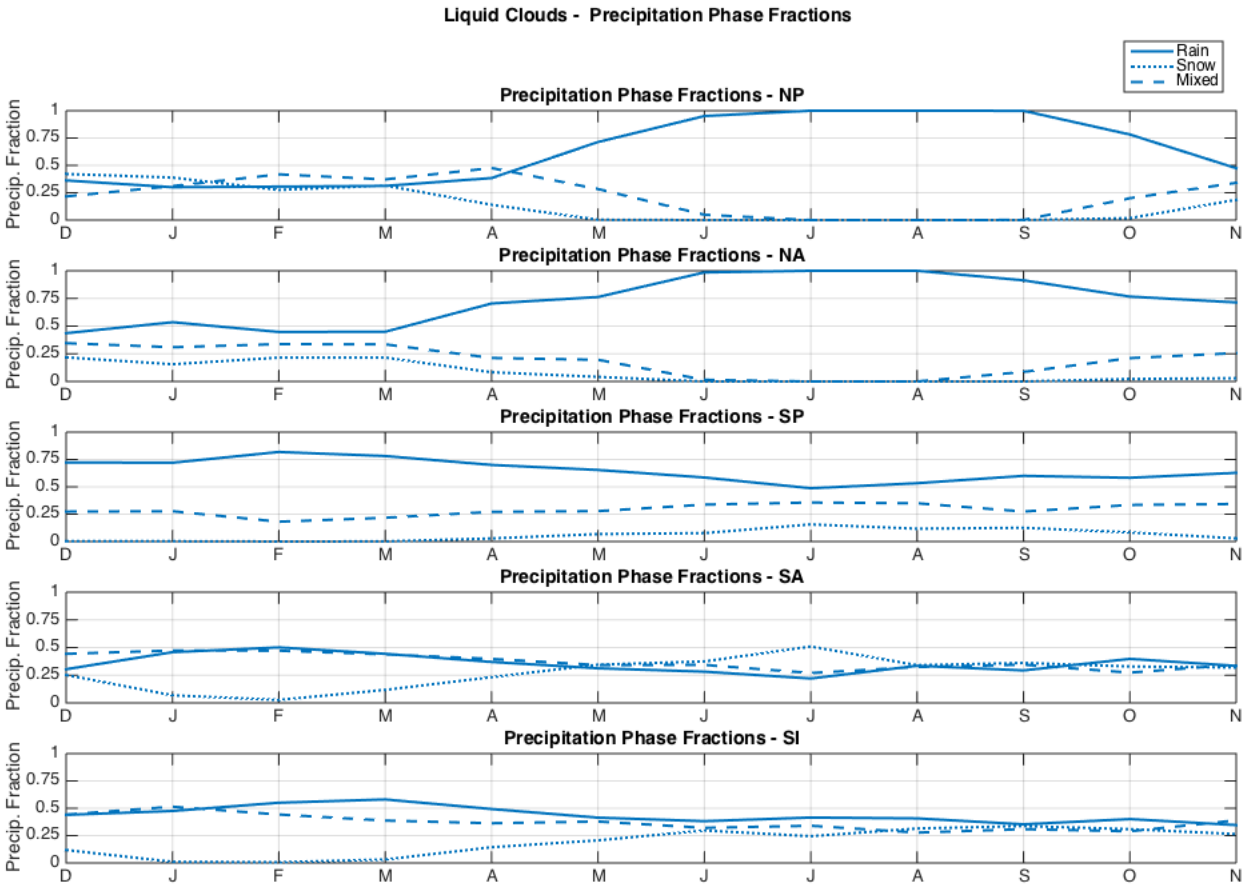

Figure 4.13: Precipitation phase fractions for each month and each marine region for all liquid water clouds. Rain, snow, and mixed phase fractions sum to one.

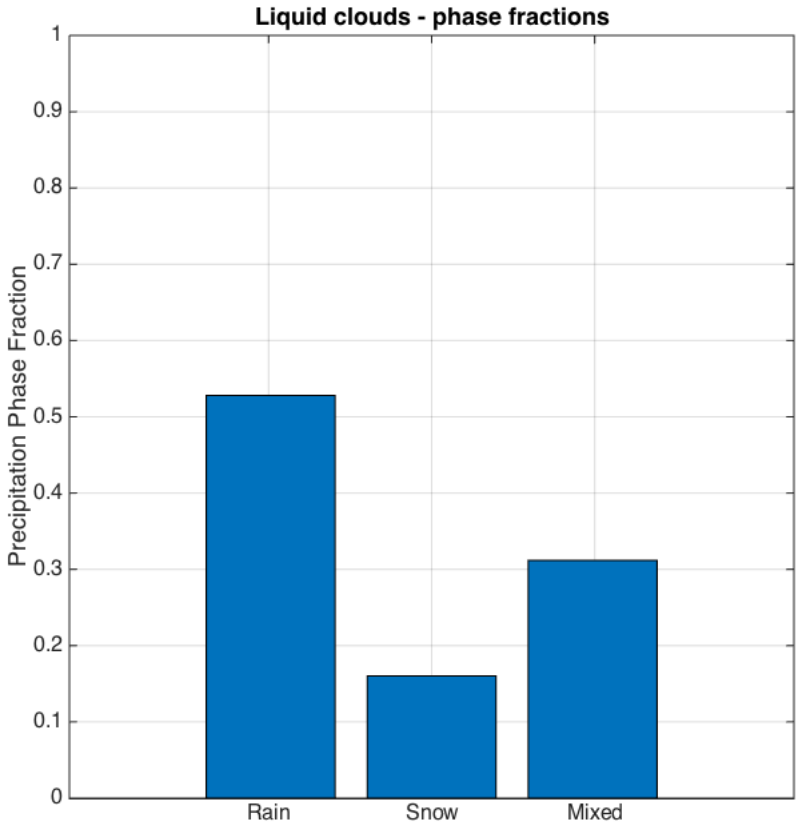

Figure 4.14: Bulk precipitation phase fractions all liquid water clouds. Counts include all marine regions and all months. Rain, snow, and mixed phase fractions sum to one.

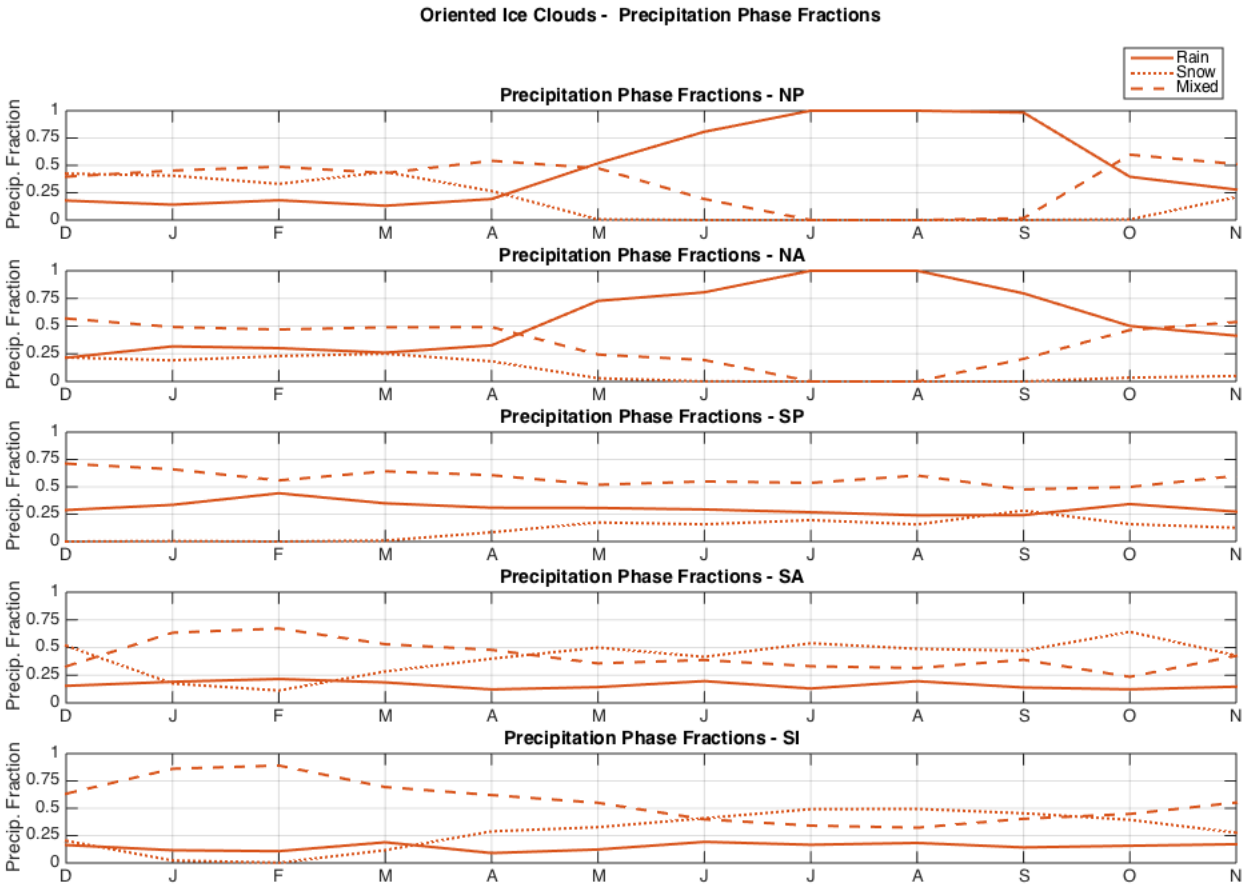

Figure 4.15: Precipitation phase fractions for each month and each marine region for all horizontally oriented ice clouds. Rain, snow, and mixed phase fractions sum to one.

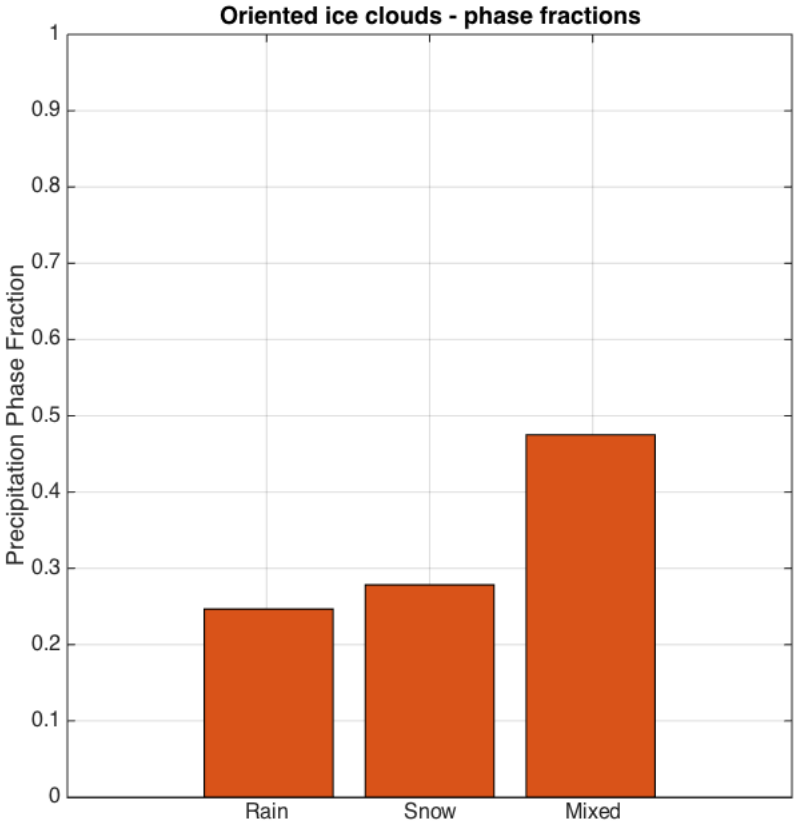

Figure 4.16: Precipitation phase fractions for each month and each marine region for all horizontally oriented ice clouds. Counts include all marine regions and all months. Rain, snow, and mixed phase fractions sum to one.

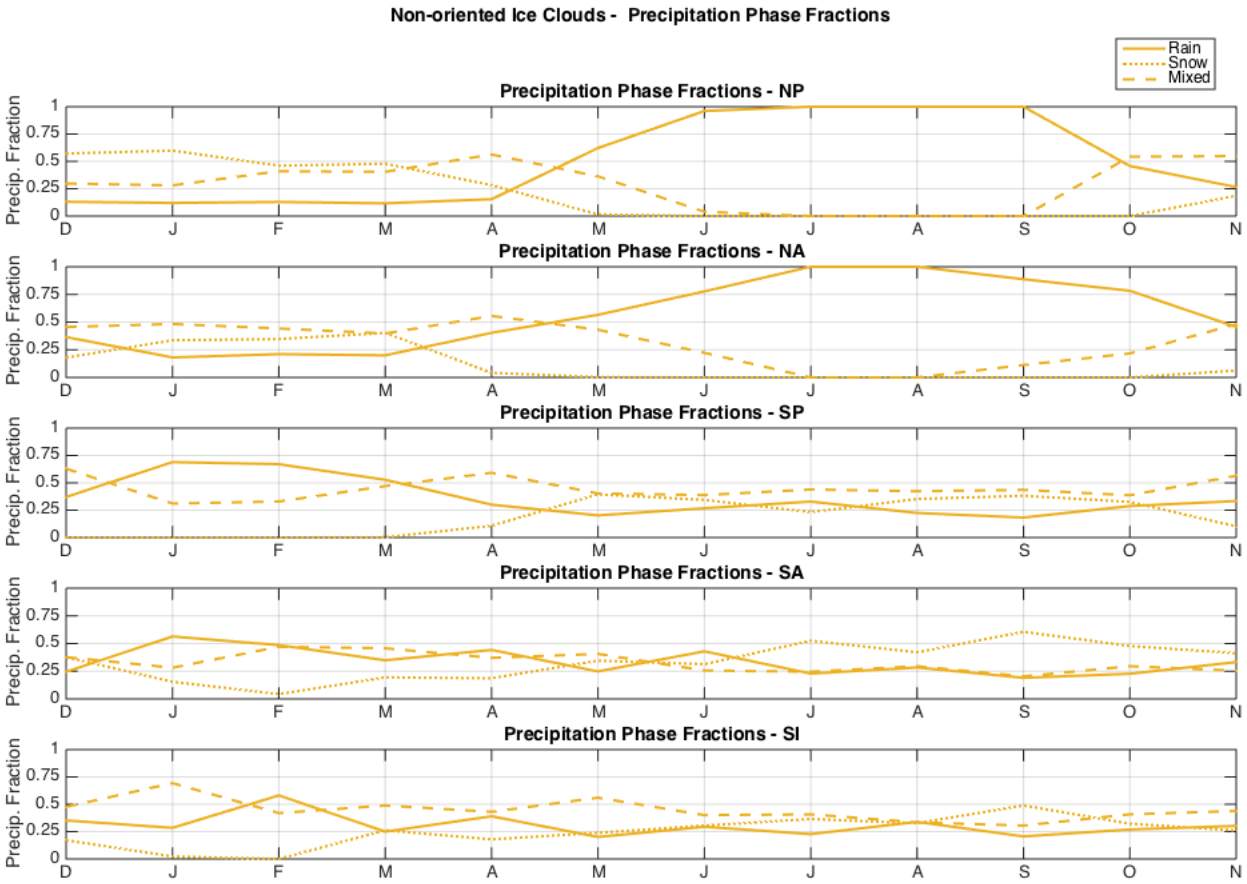

Figure 4.17: Precipitation phase fractions for each month and each marine region for all non-oriented ice clouds. Rain, snow, and mixed phase fractions sum to one.

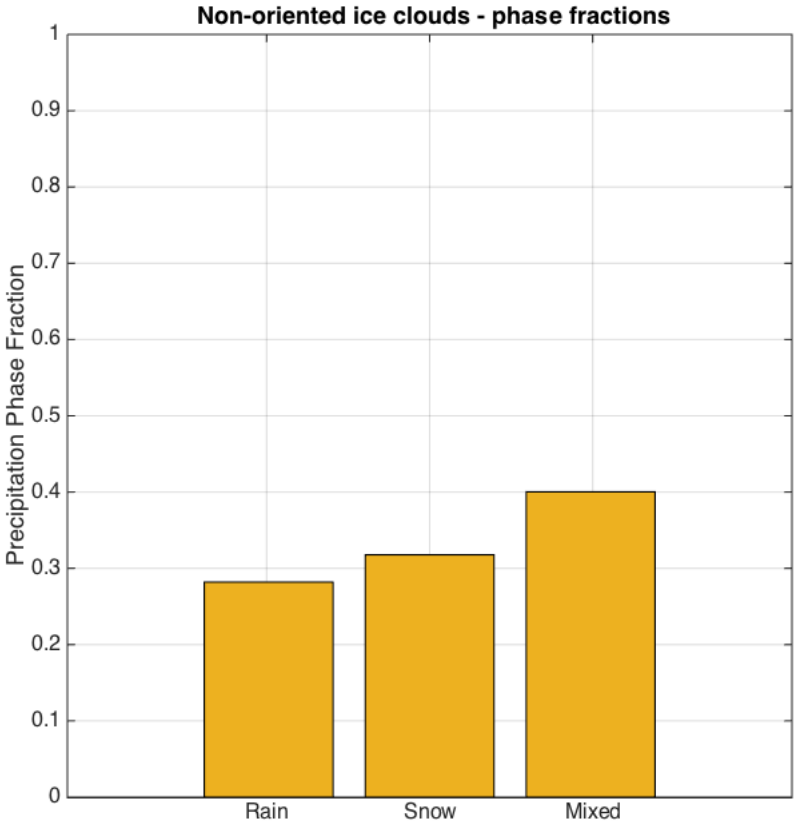

Figure 4.18: Precipitation phase fractions for each month and each marine region for all horizontally oriented ice clouds. Counts include all marine regions and all months. Rain, snow, and mixed phase fractions sum to one.

4.5.3 Ice orientation and precipitation rate

In addition to retrieving the phase of surface precipitation, CloudSat estimates the intensity of precipitation. For more details on this retrieval and the CloudSat algorithms, see Chapter 2. The results in this section focus on surface rain and surface snow rates (R_{sfc} and S_{sfc}), which are given in units mm h^{-1}. These data are obtained using a quantity called the Path Integrated Attenuation, or PIA. Precipitation rates are output of the CloudSat Precipitation Algorithm, which uses the PIA to calculate rain and snow rates. This section examines the output precipitation rates, not the raw PIA and reflectivity values, to compare precipitation intensity between the three exclusive MMM cloud phases. Raw precipitation intensity variables (PIA due to hydrometeors and maximum reflectivity) are the focus of the next section.

Bulk counts of liquid, HOIC, and NOIC clouds in all marine midlatitude mid-low cases, and for all twelve months, are considered. The cases that are counted are only those which are precipitating. Precipitation intensity fractions are partitioned into three different regimes, unique for rain and show. Within rain and snow, these fractions tell you the likelihood that a certain cloud phase type is precipitating in a light, moderate, or heavy intensity regime.

The rain and snow rates are split into three intensity regimes: *light*, *moderate*, and *heavy*. The definitions of these regimes differ from rain to snow. For **rain rates**, the regimes are as follows:

Light: $R_{\text{sfc}} < 1$ mm h^{-1}

Moderate: 1 mm h^{-1} $\leq R_{\text{sfc}} < 4$ mm h^{-1}

Heavy: $R_{\text{sfc}} \geq 4$ mm h^{-1} or $R_{\text{sfc}} < 0$ mm h^{-1}.

For **snow rates**, the regimes are defined as:

Light: $S_{\text{sfc}} < 0.25$ mm h^{-1}

Moderate: 0.25 mm $h^{-1} \leq S_{sfc} < 1$ mm h^{-1}

Heavy: $S_{sfc} \geq 1$ mm h^{-1}.

Figure 4.19 is a normalized bar plot that includes raining cases of marine midlatitude mid-low clouds only, separated by cloud phase. The fractions tell the tendency for a cloud phase to precipitate within a certain intensity range. Recall that these results are not split into months as in the previous section, but include bulk counts of all raining MMM clouds in the Northern and Southern hemispheres. These histograms are normalized such that in every figure, the same color bar will sum to one across each intensity regime. Most cloud phases tend to rain in the *light* regime. 25% or less of all cloud phases rain in the *moderate* regime. Examining heavy raining cases, it is clear that the cloud phase most likely to experience heavy rain is non-oriented ice.

Snow rate histograms for the all marine midlatitude mid-low snowing cases are shown in Figure 4.20. Almost no snow is retrieved as having rates greater than 4 mm h^{-1}, thus the change in regime definitions from rain. Roughly 90% of all snowing liquid clouds and snowing non-oriented ice clouds are light, with surface rates less than 0.25 mm h^{-1}. Most HOIC snowing clouds are very light as well. Snowing HOIC are more likely to be detected by CloudSat as moderate snowfall, compared to liquid and NOIC. In the heavy snowfall regime, the cloud with the most likelihood to snow heavily are the non-oriented cases. However, this value is still very small, less than 5%.

Overall, by examining the snowfall and rainfall rates from the CloudSat precipitation products, the most prominent takeaway is that non-oriented ice clouds are the most likely to precipitate at heavier intensities. This is especially true in the raining cases.

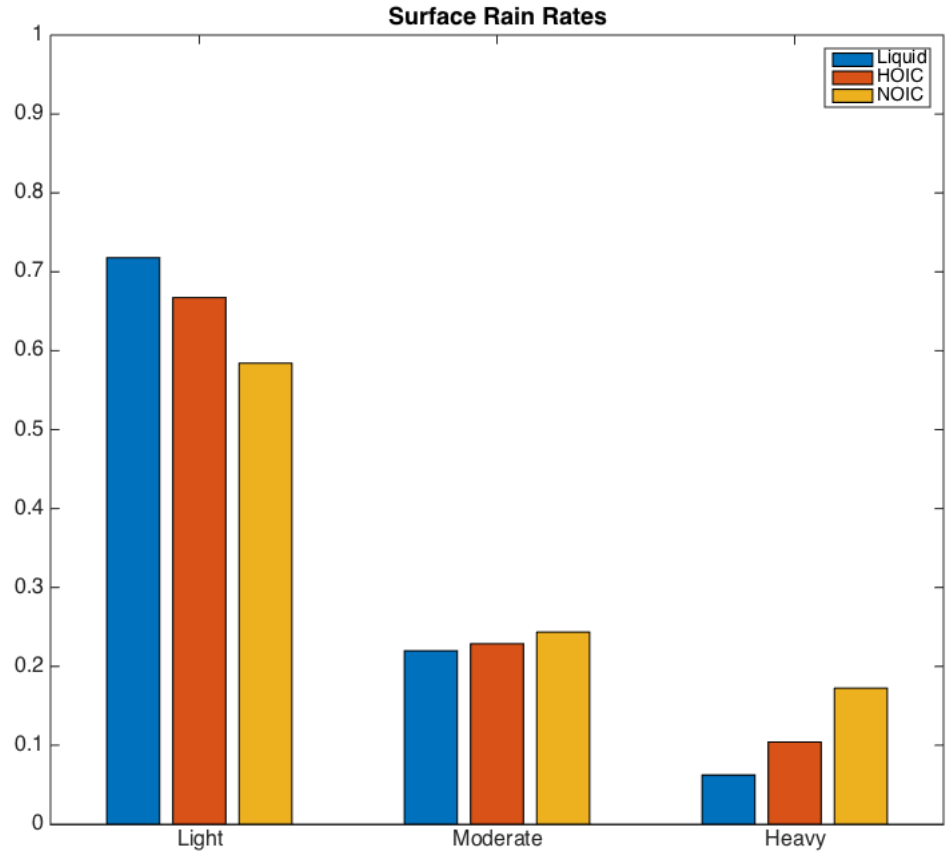

Figure 4.19: Intensities of surface rain rates for marine midlatitude mid-low clouds.

4.5.4 Ice orientation and raw precipitation intensity data

This section investigates precipitation intensity by examining the raw CloudSat reflectivity and attenuation data. Only precipitating cases are considered. Three quantities are explored: the path integrated attention, the maximum reflectivity, and the height of the maximum reflectivity. The quantities discussed here are defined as follows:

CloudSat PIA hydrometeor (dB): The path integrated attenuation due to hydrometeors in the column. Derived from the 2C-PRECIP-COLUMN file.

CloudSat Max. Reflectivity (dBz): The maximum above-surface reflectivity in the column. Cases whose maximum is above 5 km are excluded. Derived from the 2B-GEOPROF file.

CloudSat Max. Reflectivity height (km): Height at which the maximum above-surface reflectivity occurs. Cases whose maximum is above 5 km are excluded. Derived from the 2B-GEOPROF file.

We explore these quantities to further clarify any trends of cloud phases precipitating at higher or lower intensities. Figures 4.21, 4.22, and 4.23 show normalized histograms of the PIA from hydrometeors, the maximum reflectivity, and the maximum reflectivity height, respectively. Precipitating oriented ice clouds and non-oriented ice clouds are compared. Liquid water cloud retrievals are not included.

The same general interpretation seen in the previous section arises: non-oriented ice clouds are more likely to precipitate at higher "strengths" or intensities. NOIC have a higher probability of containing larger hydrometeor PIA amounts as seen in Figure 4.21. NOIC PIA values also span a wider range. Additionally, the maximum reflectivity values of precipitating NOIC cases are higher than those for HOIC cases.

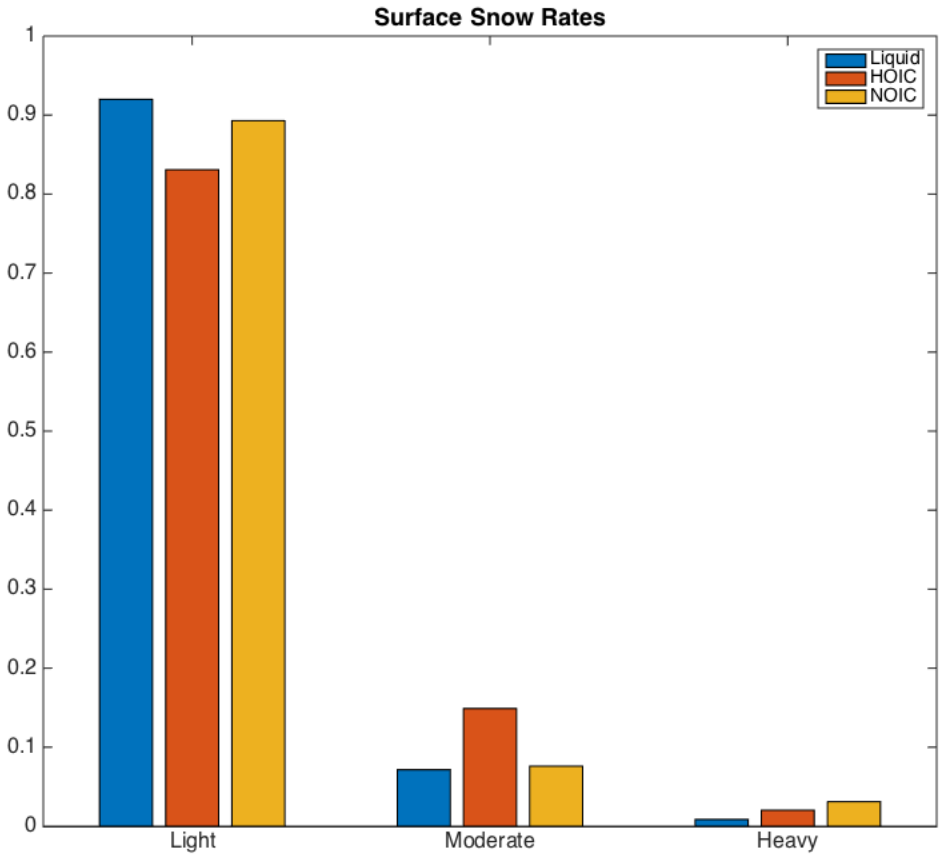

Figure 4.20: Intensities of surface snow rates for marine midlatitude mid-low clouds.

Most precipitating oriented ice cases have a maximum reflectivity value near 6 dBz. Non-oriented precipitating cases have maximum reflectivity values closer to 13 dBz. Recall that reflectivity in dBz is on a logarithmic scale, so these differences are large.

Lastly, Figure 4.23 shows the heights at which the maximum reflectivity occurs for oriented vs. non-oriented ice clouds. In the HOIC cases, maximum reflectivity values occur at lower altitudes. This point echoes that from Section 4.3, where we saw from CALIOP layer top altitude retrievals that NOIC layers reside higher than HOIC layers. Non-oriented ice retrievals not only precipitate at heavier rates, but the precipitation is often heaviest at higher altitudes. Both of these points suggest that NOIC retrievals may correspond to more turbulent clouds.

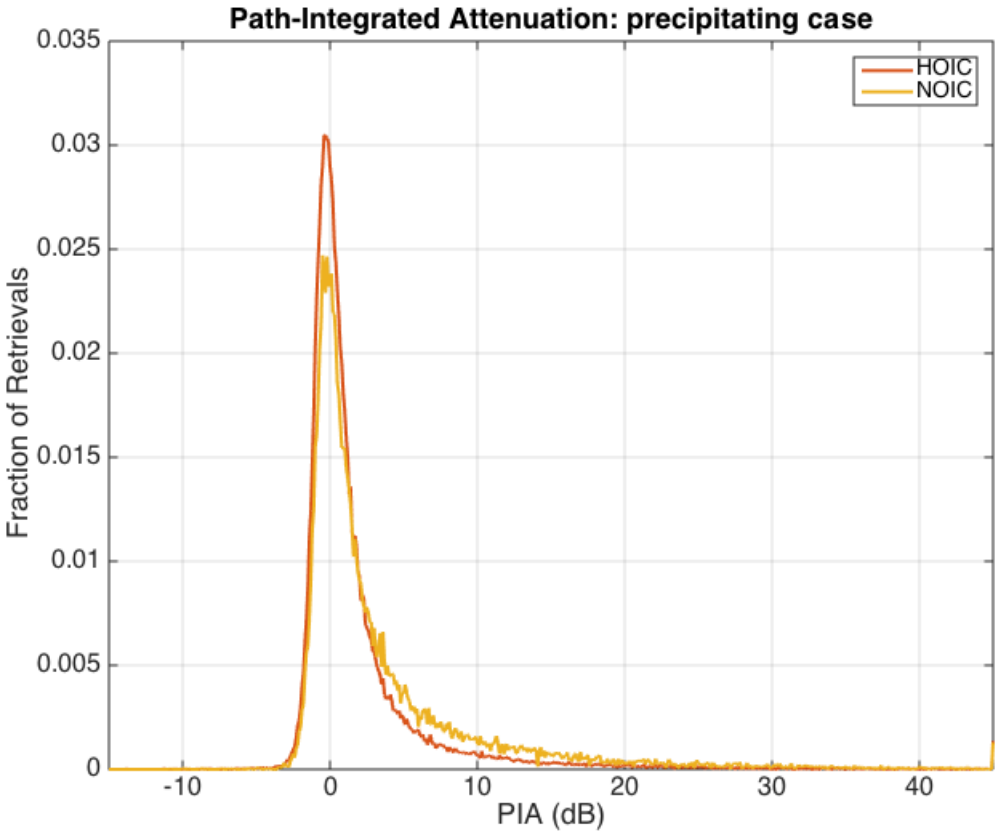

Figure 4.21: Normalized histogram of the path-integrated attenuation (dB) due to hydrometeors for precipitating fields of view. Oriented and non-oriented marine midlatitude mid-low clouds are shown.

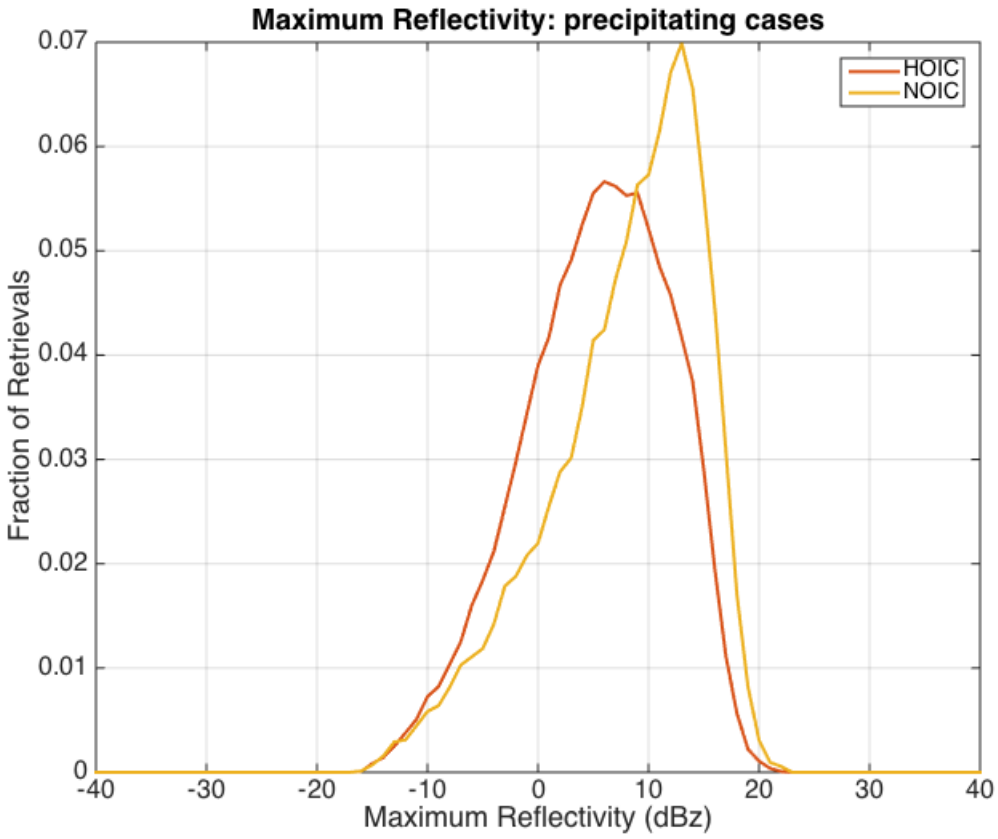

Figure 4.22: Normalized histogram of the maximum reflectivity (dBz) for precipitating fields of view. Oriented and non-oriented marine midlatitude mid-low clouds are shown. To remove ground clutter, only cases where the maximum reflectivity height is above 1.5 km and below 5 km are included.

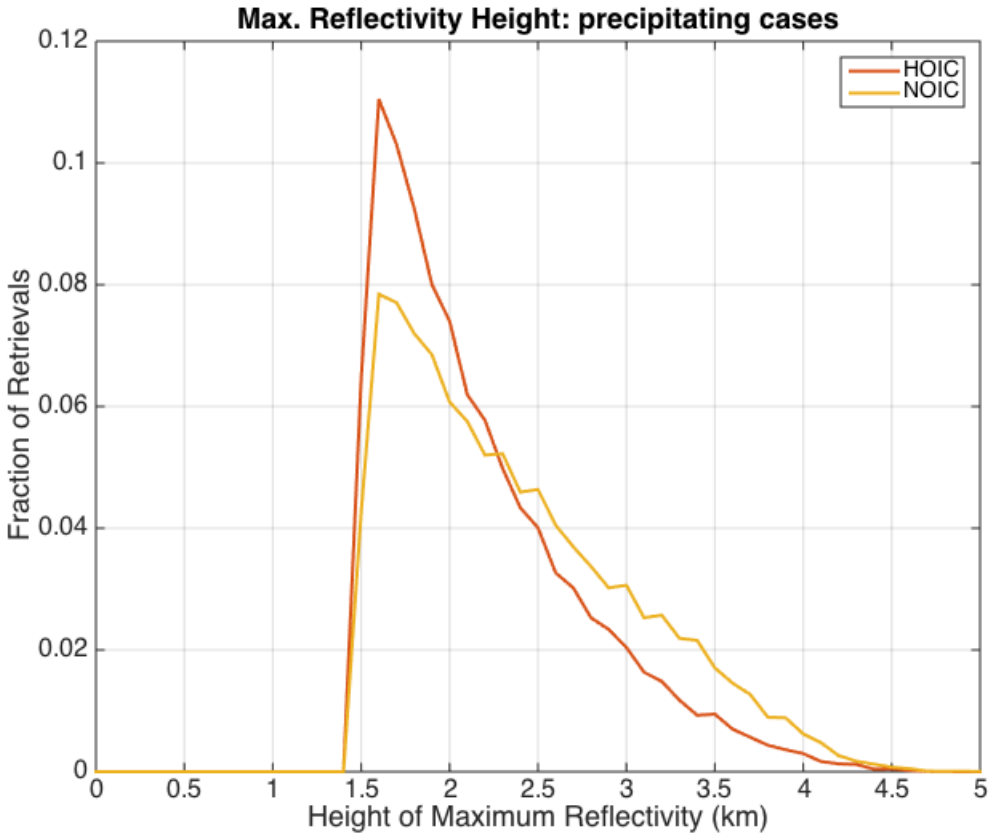

Figure 4.23: Normalized histogram of the maximum reflectivity heights f(km) for precipitating fields of view. Oriented and non-oriented marine midlatitude mid-low clouds are shown. To remove ground clutter, only cases where the maximum reflectivity height is above 1.5 km and below 5 km are included.

Chapter 5

Discussion

The collocation of CloudSat, MODIS, and CALIOP for one year of orbit has shed much light on the relationships between cloud properties observed by each instrument. Recall from the Introduction that cloud ice is not thought to be prevalent in marine *midlatitude* lower level clouds. Ice clouds are more associated with clouds at either higher altitudes or low clouds at higher latitudes (i.e. Arctic clouds). However, we have shown that low-level marine clouds contain ice quite often in marine midlatitude regions.

The CALIOP V3 phase retrievals have shown that cloud ice can actually compose up to 22% of marine midlatitude cloud retrievals in winter months as shown in Figure 4.6. Thus, ice in marine midlatitude mid-low clouds certainly deserve to be studied comprehensively. Not only does ice occur frequently in this subset of clouds, but a certain signature of oriented ice clouds has interesting correlations to other cloud properties. In fact, most winter marine midlatitude mid-low ice clouds are retrieved by CALIOP as oriented ice. Oriented ice clouds are retrieved as relatively warm in temperature, peaking near -16° C (257 K). Ice plates are known to exist at a

wide range of temperatures in clouds, anywhere from -40° C to 0° C. Oriented ice retrievals are also lower in altitude than non-oriented ice clouds (see Figure 4.8(b)). Even more interestingly, oriented ice clouds precipitate far more frequently than non-oriented ice clouds and liquid water clouds (Figure 4.11). There also seem to be significant differences in cloud properties comparing northern oceans to southern oceans. Southern oceans do not see high maximums of marine midlatitude mid-low cloud ice as is seen in the Northern oceans. The variance in ice cloud amount between Northern and Southern oceans is likely due to inherent differences in seasonal temperature variations between the two hemispheres. However, such analysis is not explored in this thesis.

Oriented ice retrievals always occur more frequently than non-oriented ice in marine midlatitude mid-low clouds. The presence of HOIC is seen strongly in the Northern Pacific cold months, specifically December 2006 through April 2007. Strong monthly averaged concentrations exist directly off of the coasts of Siberia and North America. In these Northern Pacific regions, HOIC can compose up to 18% of marine midlatitude mid-low clouds. The Northern oceans have a generally high HOIC count, only dropping below 5% for four months in June through September. High counts of HOIC are not seen in the Southern marine winters, where the maximum of HOIC fraction barely exceeds 5%. These strong differences may be inherent to basic differences between Northern and Southern Hemispheres. The North contains much more landmass, whereas the South is comprised mostly of ocean surfaces. The differences in landmasses in the Northern and Southern Hemispheres also implies that there are different concentrations of aerosols in the two hemispheres. Thus, there may be different levels of available cloud condensation nuclei and ice nuclei.

When bulk properties of HOIC and NOIC are compared, the differences in ice

orientation become more complex. Non-oriented ice tends to reside at higher altitudes within our 0-5 km range. Consequently, the layer top temperature of these cloud retrievals tend to be colder for NOIC than HOIC. HOIC retrievals have a smaller range of temperatures and center near -16° C (257 K), not much below freezing. NOIC span a much wider range of temperatures and appears bimodal. Most NOIC temperatures occur near -33° C (240 K), but can be as high as 0° C (see Figure 4.8(b)).

MODIS effective radius retrievals are based on the phase retrievals from visible channels of the spectroradiometer. Naturally, when MODIS phase is detected, it is often times done so from deeper layers of the cloud. "Deeper" is compared to the layer 1 top altitudes from CALIOP. The first CALIOP cloud layer could easily be higher in altitude than the MODIS visible cloud retrieval. The point being that MODIS cloud phase retrievals are much different than CALIOP cloud phase retrievals. The effective radius results included in Chapter 4 include only cases where both MODIS and CALIOP detect ice. This small set of retrievals tells us that oriented ice crystals are detected by MODIS with larger effective radii than NOIC. The MODIS radius retrievals are done assuming a fixed ice habit, which does not include flat plates such as those associated with HOIC. The most important results is that in low clouds, MODIS phase retrievals in general are in disagreement with CALIOP phase retrievals. Especially so for cases where CALIOP detects low level ice.

Perhaps the most exciting results shown in the previous chapter are those using the CloudSat precipitation data. The collocation of CALIOP cloud phase and CloudSat cloud and precipitation data demonstrate that HOIC retrievals are most likely to be detected as producing surface precipitation, compared to NOIC and liquid clouds. There is no intuitive reason why clouds with oriented ice crystals are

more likely to yield surface precipitation. But perhaps reason we see less surface precipitation in the non-oriented ice clouds is because CALIOP is detecting NOIC aloft, and not actually directly above the surface precipitation. In other words, if you have a precipitating cloud whose top layer is composed of ice crystals, turbulent winds may cause those ice crystals to be blown from the top of the cloud, resulting in their non-orientation. These non-oriented crystals may then not sit vertically on top of a precipitating area observed by CloudSat. Whereas in the case of oriented crystals, turbulent winds do not exist (otherwise the crystals would not be retrieved as oriented), and thus CloudSat is able to detect surface precipitation directly under the oriented crystals.

There are also slight differences between marine regions as far as what type of precipitation is most likely to occur within each cloud phase. For example, NOIC in the northern and southern cold months have a greater chance than HOIC to produce surface snow in this regions/seasons. Whereas in the South Atlantic and South Indian winters, NOIC has an equal if not lesser chance than HOIC to snow. Generally, liquid clouds are most likely to precipitate rain, HOIC are most likely to precipitate mixed phase, and NOIC are most likely to precipitate snow.

Insightful trends arise when observing CloudSat precipitation rates and intensities as well. Liquid water clouds have the highest probability of precipitating with surface rates < 0.25 mm h^{-1}. Non-oriented ice retrievals are most likely to produce heavier rain and snow at the marine surface, compared to HOIC and liquid clouds. This could connect to similar trends mentioned above, such as NOIC residing at higher cloud tops and colder temperatures. Non-oriented cases would be most likely related perhaps to turbulent cloud cases. The turbulence would prevent any of the ice from staying oriented. Also, more convective turbulent cases tend to produce heavier precipitation.

This sentiment is echoed when examining the raw path-integrated attenuation and maximum reflectivity values from CloudSat. Non-oriented ice are more likely than oriented ice to have higher hydrometeor PIA values and higher maximum reflectivity values. To summarize the correlations found between CALIOP cloud phase and all CloudSat precipitation data, refer to the table in Figure 5.1.

There is a grave need to further studied low ice-containing clouds in these marine midlatitude environments. So far, field campaigns have not captured the incidence of low ice clouds in marine midlatitude settings. Most in-situ observations of low-level ice clouds are performed in Arctic regions. As a result, cloud ice in models may be biased in their parameterizations. Further exploration of marine midlatitude low ice clouds is necessary to fully understand the cloud properties that are observed in this work. Future field campaigns may be able to validate some of the complex cloud relationships that we observe here, such as the strong correlation between oriented ice and surface precipitation. Accounting for these midlatitude ice clouds could greatly change the performance of cloud resolving models and could enhance the consistencies between cloud observations and models. Improving the cohesion between cloud models and global cloud observations may likely decrease the uncertainty in radiative energy balances that has been echoed in the two most recent IPCC reports [21].

	Liquid water clouds	Horizontally oriented ice clouds	Non-oriented ice clouds
Precipitation frequency	less than 30% of cases precipitate.	over half, up to 75% of cases precipitate.	usually less than 50%, but greater than 30% of cases precipitate.
Precipitation phase	most precipitating cases are rain.	47% of precipitating cases are mixed. more snow cases than rain.	40% of precipitating cases are snow. more mixed cases than rain.
Precipitation intensity	most precipitating cases, rain and snow, are very light in intensity.	mostly moderate and light rain rates. mostly light snow rates.	heavier rain and snow rates.

Figure 5.1: Summaries of the results correlating CALIOP cloud phase and CloudSat precipitation properties.

Chapter 6

Conclusions and future work

Marine midlatitude ice clouds occur frequently but have not been studied by dedicated field experiments. The CALIOP Version 3 phase retrieval has shown us that over 20% of marine midlatitude mid-low level clouds glaciate. Almost all of the ice is retrieved as being horizontally oriented in nature. There is a strong seasonal dependence of oriented ice clouds in the northern oceans, particularly the Northern Pacific where oriented ice occurs in up to 18% of marine low ice clouds. These oriented ice clouds are also shown to be quite warm for ice clouds, with most cloud tops measured near -16° C, only slightly below freezing.

Collocating CloudSat, CALIOP, and MODIS observations gives the ability to connect CALIOP cloud phase to other satellite retrieved cloud properties, such as particle effective radius and precipitation. There is a strong positive correlation between cloud ice orientation and surface precipitation. Oriented ice clouds are precipitating up to 78% of the time in Northern winter months. Across all marine regions and all twelve months of collocated data, HOIC retrievals are precipitating more than 50% of the time. Liquid water clouds and non-oriented ice clouds

precipitate in less than 50% of retrievals. However, another interesting correlation with CloudSat precipitating data reveals that when non-oriented ice clouds *do* precipitate, it is with higher intensities. This is the case especially with surface rain rates. Oriented ice clouds and liquid water clouds tend to precipitate with lower intensities.

The research covered in this thesis has shed light both on cloud properties and the instruments used to retrieve them. Space satellite data retrievals have the advantage of viewing full global coverage, but there are disadvantages as well. Problems arise when developing data algorithms aim to observe low cloud properties and surface precipitation. Near-surface events such as low clouds and precipitation can become difficult to detect accurately with satellites. This research is only a part of the contribution to improve cohesion between cloud observations and modeling. Integrating the results presented here into cloud resolving models could improve our understanding between cloud-atmosphere interactions, especially above oceans which cover most of the Earth's surface.

Collocating the instruments helps to validate cloud cases across MODIS, CALIOP, and CloudSat, in addition to providing new and original matched datasets. These matched data allow us to connect and correlate certain cloud properties that could not previously be connected. Each instrument has different sensitivities. Combining the instruments gives one of the most spectrally and spatially comprehensive view of clouds at all latitudes. The findings on marine midlatitude clouds in this research are summarized here, as well as what can be done in the future to continue this work.

6.1 Conclusions

Evidence presented in this thesis shows that ice clouds in marine midlatitude environments can exist close to the surface. The significant amount of near-surface (cloud top $<$ 5 km) cloud ice has only been examined in arctic regions until now. Clearly, middle to low level clouds are worth examining on a global scale across a large temporal range. In this thesis we focus on such clouds during twelve month period from December 2006 to November 2007 by using a combination of three remote sensing instruments. This specific time range assures the ability to observe oriented ice crystals with CALIOP. Such a time period includes data only when CALIOP's viewing angle was pointed at 0.3° off nadir, allowing for specular reflection. The collocation between CloudSat, MODIS, and CALIOP allows us to draw statistics for the year's worth of A-Train orbit. We focus on midlatitude oceans with low cloud cases.

Unique relationships arise when comparing between CALIOP cloud phase and other cloud properties. The cloud properties aside from phase type examined here are: cloud top altitude, temperature, cloud particle effective radius, precipitation incidence, precipitation phase, and precipitation intensity. Such relationships have never been observed with non-spaceborne instruments, the collocation of these cross-platform data have given us the opportunity to explore these relationships and more. Observations of midlatitude marine clouds is vital. Field experiments do not capture these complex cloud processes that we observe with satellites. The spatial range of space satellites provides consistent data with incomparable spatial coverage.

Most cloud microphysical models depend on in-situ data for validation. In-situ observations detect cloud particles at a close scale, as opposed to remote sensing which observes microphysics from very high ranges in space. If cloud models rely

solely on ground based or near-ground observations to validate cloud properties, then spatial coverage of clouds captured by the remote sensors' capabilities are excluded from cloud model development entirely.

Such a lack of consistency between comprehensive cloud observations and cloud models is well known in the atmospheric community. This topic is discussed in the 2007 and 2013 IPCC reports. Clouds play a huge role in radiative effects and marine clouds are often above much of the Earth's surface. Until a consistency between observational platforms and cloud modeling is fully realized, our cloud modeling capabilities will lack the complexity that the atmosphere experiences.

6.2 Future work

There is very large potential as to the amount of cloud and aerosol information that can be gathered using the collocated dataset presented in this thesis. There are a number of topics that could be explored with the current dataset that are not included in this research but will be mentioned in this section. The time permitted in a master's degree program did not allow for a complete analysis of all available data. However, continuing research at the Cooperative Institute for Meteorological Satellite Studies will shed light on issues that are not covered in this thesis.

The output collocated files also contain, for example, aerosol optical depth products from MODIS. MODIS AOD values may or may not provide insight into what could be nucleating ice in these marine midlatitude mid-low clouds. However, the problem may arise that cloud events cause cloud-contamination in the aerosol data. Thus, aerosol retrievals from both MODIS and CALIOP in cloudy cases may not be valid.

What could also provide insight into aerosol data is collocated aerosol forecasting

models. Aerosol modeling is currently performed at the Navy Research Laboratory under Dr. Jeff Reid. Collocating aerosol model data with the satellite observations may shed light on how HOIC and NOIC become nucleated. Differences in available ice nuclei surely exist between the northern and southern oceans. This is caused by differences in landmass between north and south hemispheres. These differences in ice nucleation may lead to differences in ice habits.

Further work may also include cloud modeling studies that attempt to produce oriented ice crystals in precipitating clouds. Utilizing cloud microphysical modeling may help explain why certain cloud features correspond to surface precipitation features (e.g. non-oriented ice clouds having a greater tendency to snow than oriented ice clouds). Cloud resolving models will allow for better understanding of these relationships.

Another large part of these low level ice clouds that are detected by CALIOP as ice below 5 km is whether or not ice exists lower within the cloud layer. The results in this research include CALIOP phase retrievals only in the first layer. Beyond the first layer could easily be liquid water in the cloud. This adds a level of complexity to our subset of low level marine midlatitude clouds. Ice orientation and thickness of ice into the cloud depth may also correlate to precipitation properties.

Clearly, the vertical resolution of CALIOP could be further taken advantage of to gain higher knowledge about these cloud layers. Such is the case with CloudSat as well. Vertical profiles of precipitation data from CloudSat can also be explored, such as above-surface precipitation. Recall that all of the results in Chapter 4 included CloudSat surface precipitation. Whether precipitation exists higher in the atmospheric column may be related to differences in higher cloud phase.

Appendix

The following tables detail which data products from each instrument are included in the output matched files. The data are listed in the order of MODIS, CloudSat, CALIOP cloud layer, and CALIOP aerosol layer products. The file from which the data originated is also listed as well as a data description or attribute.

MODIS data name	**Origin file**	**Description**
MODIS Latitude	MYD03	MODIS Latitude
MODIS Longitude	MYD03	MODIS Longitude
MODIS Time	MYD03	MODIS Time
Land Sea Mask	MYD03	MODIS averaged Land/Sea Mask. Original integer mask: 0 - Shallow Ocean (Ocean 5k from coast OR 50m deep). 1 - Land (not anything else). 2 - Ocean Coastlines and Lake Shorelines. 3 - Shallow Inland Water. 4 - Ephemeral (intermittent) Water. 5 - Deep Inland Water. 6 - Moderate or Continental Ocean. 7 - Deep Ocean.
Day Night Mask	MYD03	MODIS averaged Day/Night Mask. Original integer mask: 0 - night. 1 - day.
Cloud Top Height	MYD06	Aqua MODIS Averaged Cloud Top Height (m).

Cloud Top Height Std	MYD06	Standard deviation of Cloud Top Height (m).
Cloud Top Pressure	MYD06	Cloud Top Pressure Level (rounded to nearest 5 mb) (hPa). Scale by 0.1.
Cloud Top Temp	MYD06	MODIS cloud top temperature (K). Scale by 0.01.
Cloud Top Temp Std	MYD06	Standard deviation of cloud top temperature (K). Scale by 0.01.
Cloud Emissivity	MYD06	Cloud Effective Emissivity from Cloud Top Pressure Retrieval. Scale by 0.01.
Cloud Emissivity Std	MYD06	Standard deviation of Cloud Effective Emissivity from Cloud Top Pressure Retrieval. Scale by 0.01.
Cloud Fraction	MYD06	MODIS derived cloud fraction.
50% Ice Fraction	MYD06	MODIS derived ice fraction.
Liquid Fraction	MYD06	MODIS derived liquid water fraction.
Cloud OT	MYD06	Aqua MODIS Averaged Cloud Optical Thickness. No uncertainty restrictions. Scale by 0.01.
Cloud OT Std	MYD06	Standard deviation of Cloud Optical Thickness. No uncertainty restrictions. Scale by 0.01.
Cloud OT Good	MYD06	Averaged Cloud Optical Thickness. Only points with uncertainty 50%. Scale by 0.01.
Cloud OT Good Std	MYD06	Standard deviation of Cloud Optical Thickness. Only points with uncertainty 50%. Scale by 0.01.
Cloud OT Better	MYD06	Averaged Cloud Optical Thickness. Only points with uncertainty 20%. Scale by 0.01.
Cloud OT Better Std	MYD06	Standard deviation of Cloud Optical Thickness. Only points with uncertainty 20%. Scale by 0.01.
Cloud OT Best PCL	MYD06	Averaged Cloud Optical Thickness including points identified as either partly cloudy from 250m cloud mask test or 1km cloud edges. Only points with uncertainty 10%. Scale by 0.01.

Cloud OT Best PCL Std	MYD06	Standard deviation of Cloud Optical Thickness including points identified as either partly cloudy from 250m cloud mask test or 1km cloud edges. Only points with uncertainty 10%. Scale by 0.01.
Ice Effective Radius	MYD06	Effective radius for ice particles, excluding points identified as either partly cloudy from 250m cloud mask test or 1km cloud edges. No restraints on uncertainty.
Ice Effective Radius Std	MYD06	Standard deviation of effective radius for ice particles, excluding points identified as either partly cloudy from 250m cloud mask test or 1km cloud edges. No restraints on uncertainty.
Ice Effective Radius Good	MYD06	Effective radius for ice particles, excluding points identified as either partly cloudy from 250m cloud mask test or 1km cloud edges. Only points with uncertainty 50%.
Ice Effective Radius Good Std	MYD06	Standard deviation of effective radius for ice particles, excluding points identified as either partly cloudy from 250m cloud mask test or 1km cloud edges. Only points with uncertainty 50%.
Ice Effective Radius Better	MYD06	Effective radius for ice particles, excluding points identified as either partly cloudy from 250m cloud mask test or 1km cloud edges. Only points with uncertainty 20%.
Ice Effective Radius Better Std	MYD06	Standard deviation of effective radius for ice particles, excluding points identified as either partly cloudy from 250m cloud mask test or 1km cloud edges. Only points with uncertainty 20%.
Ice Effective Radius Best	MYD06	Standard deviation of effective radius for ice particles, excluding points identified as either partly cloudy from 250m cloud mask test or 1km cloud edges. Only points with uncertainty 10%.
Ice Effective Radius Best Std	MYD06	Standard deviation of effective radius for ice particles, excluding points identified as either partly cloudy from 250m cloud mask test or 1km cloud edges. Only points with uncertainty 10%.

Liquid Effective Radius	MYD06	Effective radius for liquid particles, excluding points identified as either partly cloudy from 250m cloud mask test or 1km cloud edges. No restraints on uncertainty.
Liquid Effective Radius Std	MYD06	Standard deviation of effective radius for liquid particles, excluding points identified as either partly cloudy from 250m cloud mask test or 1km cloud edges. No restraints on uncertainty.
Liquid Effective Radius Good	MYD06	Effective radius for liquid particles, excluding points identified as either partly cloudy from 250m cloud mask test or 1km cloud edges. Only points with uncertainty 50%.
Liquid Effective Radius Good Std	MYD06	Standard deviation of effective radius for liquid particles, excluding points identified as either partly cloudy from 250m cloud mask test or 1km cloud edges. Only points with uncertainty 50%.
Liquid Effective Radius Better	MYD06	Effective radius for liquid particles, excluding points identified as either partly cloudy from 250m cloud mask test or 1km cloud edges. Only points with uncertainty 20%.
Liquid Effective Radius Better Std	MYD06	Standard deviation of effective radius for liquid particles, excluding points identified as either partly cloudy from 250m cloud mask test or 1km cloud edges. Only points with uncertainty 20%.
Liquid Effective Radius Best	MYD06	Effective radius for liquid particles, excluding points identified as either partly cloudy from 250m cloud mask test or 1km cloud edges. Only points with uncertainty 10%.
Liquid Effective Radius Best Std	MYD06	Standard deviation of effective radius for liquid particles, excluding points identified as either partly cloudy from 250m cloud mask test or 1km cloud edges. Only points with uncertainty 10%.
Ice Effective Radius PCL	MYD06	Effective radius for ice particles, including points identified as either partly cloudy from 250m cloud mask test or 1km cloud edges. No restraints on uncertainty.

Ice Effective Radius Good PCL	MYD06	Effective radius for ice particles, including points identified as either partly cloudy from 250m cloud mask test or 1km cloud edges. Only points with uncertainty 50%.
Ice Effective Radius Better PCL	MYD06	Effective radius for ice particles, including points identified as either partly cloudy from 250m cloud mask test or 1km cloud edges. Only points with uncertainty 20%.
Ice Effective Radius Best PCL	MYD06	Effective radius for ice particles, including points identified as either partly cloudy from 250m cloud mask test or 1km cloud edges. Only points with uncertainty 10%.
Ice Effective Radius PCL Std	MYD06	Standard deviation of effective radius for ice particles, including points identified as either partly cloudy from 250m cloud mask test or 1km cloud edges. No restraints on uncertainty.
Ice Effective Radius Good PCL Std	MYD06	Standard deviation of effective radius for ice particles, including points identified as either partly cloudy from 250m cloud mask test or 1km cloud edges. Only points with uncertainty 50%.
Ice Effective Radius Better PCL Std	MYD06	Standard deviation of effective radius for ice particles, including points identified as either partly cloudy from 250m cloud mask test or 1km cloud edges. Only points with uncertainty 20%.
Ice Effective Radius Best PCL Std	MYD06	Standard deviation of effective radius for ice particles, including points identified as either partly cloudy from 250m cloud mask test or 1km cloud edges. Only points with uncertainty 10%.
Liquid Effective Radius PCL	MYD06	Effective radius for liquid particles, including points identified as either partly cloudy from 250m cloud mask test or 1km cloud edges. No restraints on uncertainty.
Liquid Effective Radius Good PCL	MYD06	Effective radius for liquid particles, including points identified as either partly cloudy from 250m cloud mask test or 1km cloud edges. Only points with uncertainty 50%.

Liquid Effective Radius Better PCL	MYD06	Effective radius for liquid particles, including points identified as either partly cloudy from 250m cloud mask test or 1km cloud edges. Only points with uncertainty 20%.
Liquid Effective Radius Best PCL	MYD06	Effective radius for liquid particles, including points identified as either partly cloudy from 250m cloud mask test or 1km cloud edges. Only points with uncertainty 10%.
Liquid Effective Radius PCL Std	MYD06	Standard deviation of effective radius for liquid particles, including points identified as either partly cloudy from 250m cloud mask test or 1km cloud edges. No restraints on uncertainty.
Liquid Effective Radius Good PCL Std	MYD06	Standard deviation of effective radius for liquid particles, including points identified as either partly cloudy from 250m cloud mask test or 1km cloud edges. Only points with uncertainty 50%.
Liquid Effective Radius Better PCL Std	MYD06	Standard deviation of effective radius for liquid particles, including points identified as either partly cloudy from 250m cloud mask test or 1km cloud edges. Only points with uncertainty 20%.
Liquid Effective Radius Best PCL Std	MYD06	Standard deviation of effective radius for liquid particles, including points identified as either partly cloudy from 250m cloud mask test or 1km cloud edges. Only points with uncertainty 10%.
AOD unfiltered	MYD04	Aqua MODIS Aerosol Optical Depth with no quality flag applied
AOD good	MYD04	Aqua MODIS Aerosol Optical Depth with quality flag applied - good
AOD better	MYD04	Aqua MODIS Aerosol Optical Depth with quality flag applied - better
AOD best	MYD04	Aqua MODIS Aerosol Optical Depth with quality flag applied - best
Angstrom Exponent 1	MYD04	Angstrom exponent: 0.55/0.86 μm.

Angstrom Exponent 2	MYD04	Angstrom exponent: 0.86/2.1 μm.

CloudSat data name	**Origin file**	**Description**
CloudSat Latitude	1B CPR	CloudSat Latitude
CloudSat Longitude	1B CPR	CloudSat Longitude
CloudSat Time	1B CPR	CloudSat Time
Maximum Reflectivity	2B GEOPROF	Maximum above ground reflectivity. Surface is filtered using the Surface Height Bin. Maximum reflectivity is found by filtering out surface bin - 3.
Maximum Reflectivity Height	2B GEOPROF	Height at which the maximum above ground reflectivity occurs (m).
Cloud Top Height	1B CPR	CloudSat derived cloud top height (m) from cloud mask. Maximum height at which cloud mask = 40.
Precip. Flag	2C PRECIP COLUMN	CloudSat Precipitation flag. 0 - no precipitation detected. 1 - possible rain. 2 - probably rain. 3 - certain rain. 4 - possible snow. 5 - certain snow. 6 - possible mixed. 7 - certain mixed. 9 - uncertain.
Status Flag	2C PRECIP COLUMN	CloudSat retrieval status. 0 - both the quantitative precip rate and occurrence retrievals were successful. 1 - only the precip occurrence retrieval was successful; no precip rate was retrieved. 12-19 indicate an error condition occurred.
Convective Stratiform Flag	2C PRECIP COLUMN	Classification of rain into convective, stratiform, or shallow based on rain top height. 0 - no certain precipitation present. 1 - convective precipitation. 2 - stratiform precipitation. 3 - shallow precipitation
Surface Wind Speed	2C PRECIP COLUMN	The surface wind speed; from ECMWF (m/s).
Sea Surface Temperature	2C PRECIP COLUMN	Sea Surface Temperature (from ECMWF).

Precipitation Rate	2C PRECIP COLUMN	Precipitation rate [mm/hr]. If the maximum retrievable precipitation rate is encountered, Precip. rate is set to a negative number. The absolute value of this number is the minimum precipitation rate for the profile; the actual precipitation rate is probably higher (and may be much higher).
Freezing Level	2C PRECIP COLUMN	The height of the freezing level; from ECMWF (km). -8 corresponds to below surface.
Rain Top Height	2C PRECIP COLUMN	Estimated maximum height at which liquid precipitation is found in the column (km).
Frozen Precip. Height	2C PRECIP COLUMN	The maximum height reached by frozen precipitation (km).
PIA hydrometeor	2C PRECIP COLUMN	Two-way path integrated attenuation due to hydrometeors between the satellite and the surface (dB).
PIA near surface	2C PRECIP COLUMN	Two-way path integrated attenuation due to hydrometeors between the satellite and the lowest range bin the CPR can observe (dB).
PIA uncertainty	2C PRECIP COLUMN	Uncertainty in path integrated attenuation estimate (dB).
Melted Fraction	2C PRECIP COLUMN	The total mass fraction of liquid water contained in surface precipitation.
Rain Rate	2C PRECIP COLUMN	CloudSat surface rain rate (mm/hr). Negative rain rates indicate a high rain rate where the radar signal has been saturated. In this situation the absolute value of the rain rate should be interpreted as the minimum possible rain rate.
Rain Status	2C PRECIP COLUMN	Status indicating the retrieval method used for the rain intensity estimate.
Modeled PIA Hydrometeor	2C PRECIP COLUMN	The PIA from hydrometeors (cloud/rain/ice) that is modeled by the algorithm. This quantity does not include a multiple scattering correction. To compare this quantity to the observed PIA one most subtract the surface MS correction variable.

Surface MS Correction	2C PRECIP COLUMN	The multiple-scattering correction at the surface that is modeled by the algorithm. This quantity should be added to the modeled hydrometeor PIA to derive the uncorrected hydrometeor PIA.
Precipitable Water Content Uncertainty	2C RAIN PROFILE	1-sigma uncertainty in the precipitation (liquid + ice) water content.
Rain Quality Flag	2C RAIN PROFILE	Flag indicating the quality of the rain rate estimate. Flagging is based on the modeled multiple scattering correction, estimate of the uncertainty in the Path Integrated Attenuation (PIA) and the magnitude of the estimated PIA. Increasing values of confidence are indicative of lower uncertainty in the PIA and smaller multiple scattering effects. -1 = missing data input or land surface. 0 = no confidence. 1 = very low confidence. 2 = low confidence. 3 = moderate confidence. 4 = high confidence.
Rain Rate Uncertainty	2C RAIN PROFILE	1-sigma uncertainty estimate in the surface rain rate.
Liquid Water Content Integrated	2C RAIN PROFILE	Liquid precipitation water content, column integrated (g/m^3).
Ice Water Content Integrated	2C RAIN PROFILE	Ice precipitation water content, column integrated (g/m3).
Snow Rate Status	2C SNOW PROFILE	A one-byte (8-bit) field for retrieval status flags. The following table gives the bit position and the condition indicated if that bit is set. The table starts from the least significant bit (position 0).
Snow Rate Surface	2C SNOW PROFILE	Surface snowfall rate in mm of liquid water per hour.
Snow Rate Surface Uncertainty	2C SNOW PROFILE	Uncertainty in snowfall rate.
Snow Water Content Integrated	2C SNOW PROFILE	Total snow water content, column integrated
Layer Base Altitudes	2C RAIN PROFILE	Altitudes of five CloudSat layers (m).

Layer Top Altitudes	2C RAIN PROFILE	Altitudes of five CloudSat layers (m).
Snow Rate Layer	2C SNOW PROFILE	Snowfall rates for layers in the precipitating column in mm of liquid water per hour.
Liquid Water Content Layer	2C RAIN PROFILE	Liquid precipitation water content, layer integrated [g m^{-3}].
Ice Water Content Layer	2C RAIN PROFILE	Ice precipitation water content, layer integrated [g m^{-3}].
Snow Rate Uncertainty Layer	2C SNOW PROFILE	CloudSat estimated 1-sigma uncertainties of the snowfall rates in the precipitating column.
Snow Log N0 Layer	2C SNOW PROFILE	Retrieved log(N0) for layers for the precipitating column, where log() is common logarithm and N0 is the intercept of the assumed exponential snow particle size distribution in m-3 mm-1.
Snow Log N0 Layer Uncertainty	2C SNOW PROFILE	Uncertainty of log(N0)
Snow Log Lambda Layer	2C SNOW PROFILE	Retrieved log(λ) for layers for the precipitating column, where log(x) is common base 10 logarithm and lambda is the slope of the assumed exponential snow particle size distribution in $mm^{-}1$.
Snow Log Lambda Layer Uncertainty	2C SNOW PROFILE	Uncertainty of log(λ).
Snow Water Content Layer	2C SNOW PROFILE	Snow water content in the precipitating column [g m^{-3}]. Integrated for each layer.
Snow Water Content Layer Uncertainty	2C SNOW PROFILE	Uncertainty of snow water content by each layer.

CALIOP data name	**Origin file**	**Description**
CALIOP Latitude	CALIOP Level 1B Profile	CALIOP Latitude

CALIOP Longitude	CALIOP Level 1B Profile	CALIOP Longitude
CALIOP Time	CALIOP Level 1B Profile	CALIOP Time
Cloud Layer Top Altitude	CALIOP Level 2 Cloud Layer	Cloud layer level top altitude (km).
Cloud Layer Top Altitude Std	CALIOP Level 2 Cloud Layer	Standard deviation of cloud layer level top altitude (km).
Cloud Layer Base Altitude	CALIOP Level 2 Cloud Layer	Cloud layer level base altitude (km).
Cloud Layer Base Altitude Std	CALIOP Level 2 Cloud Layer	Standard deviation of cloud layer level base altitude (km)
Cloud Layer Top Pressure	CALIOP Level 2 Cloud Layer	Cloud layer level top pressure (hPa).
Cloud LayeCloudr Base Pressure	CALIOP Level 2 Cloud Layer	Cloud layer level base pressure (hPa).
Cloud Layer Top Temperature	CALIOP Level 2 Cloud Layer	Cloud layer level top temperature (degrees C).
Cloud Layer Top Temperature Std	CALIOP Level 2 Cloud Layer	Standard deviation of cloud layer level top temperature (degrees C).
Cloud Layer Base Temperature	CALIOP Level 2 Cloud Layer	Cloud layer level top temperature (degrees C).
Cloud Layer Base Temperature Std	CALIOP Level 2 Cloud Layer	Standard deviation of cloud layer level top temperature (degrees C).
Cloud Midlayer Temperature	CALIOP Level 2 Cloud Layer	Cloud midlayer temperature (degrees C).
Cloud Midlayer Temperature Std	CALIOP Level 2 Cloud Layer	Standard deviation of cloud midlayer temperature (degrees C).
Cloud Midlayer Pressure	CALIOP Level 2 Cloud Layer	Cloud midlayer Pressure (hPa).
Cloud Cloud Fraction	CALIOP Level 2 Cloud Layer	CALIOP layer cloud fraction.

Cloud Ice Fraction	CALIOP Level 2 Cloud Layer	CALIOP layer ice fraction.
Cloud Liq Fraction	CALIOP Level 2 Cloud Layer	CALIOP liquid fraction
Cloud Oriented Fraction	CALIOP Level 2 Cloud Layer	CALIOP oriented ice fraction.
Cloud Ice Water QA	CALIOP Level 2 Cloud Layer	CALIOP phase QA (to be applied to ice fraction and oriented fraction)
Cloud Feature Type QA	CALIOP Level 2 Cloud Layer	CALIOP feature type QA (to be applied to cloud fraction).
Cloud Lidar Ratio Initial 532	CALIOP Level 2 Cloud Layer	Cloud layer Lidar Ratio Initial 532
Cloud Lidar Ratio Final 532	CALIOP Level 2 Cloud Layer	Cloud layer Lidar Ratio Final 532
Cloud Feature Optical Depth 532	CALIOP Level 2 Cloud Layer	Cloud layer Feature Optical Depth 532
Cloud Feature Optical Depth 532 Std	CALIOP Level 2 Cloud Layer	Standard deviation of cloud layer Feature Optical Depth 532
Cloud Color Ratio	CALIOP Level 2 Cloud Layer	Cloud layer Color Ratio
Cloud Integrated Attenuated Backscatter 1064	CALIOP Level 2 Cloud Layer	Cloud layer Integrated Attenuated Backscatter 1064
Cloud Integrated Attenuated Backscatter 532	CALIOP Level 2 Cloud Layer	Cloud layer Integrated Attenuated Backscatter 532
Cloud Column Optical Depth Stratospheric 1064	CALIOP Level 2 Cloud Layer	Cloud layer Column Optical Depth Stratospheric 1064
Cloud Column Optical Depth Stratospheric 1064 Std	CALIOP Level 2 Cloud Layer	Std. deviation of cloud layer Column Optical Depth Stratospheric 1064
Cloud Column Optical Depth Stratospheric 532	CALIOP Level 2 Cloud Layer	Cloud Layer Column Optical Depth Stratospheric 532

Cloud Column Optical Depth Stratospheric 532 Std	CALIOP Level 2 Cloud Layer	Std. deviation of Column Optical Depth Stratospheric 532
Cloud Column Optical Depth Cloud 532	CALIOP Level 2 Cloud Layer	Cloud layer Column Optical Depth Cloud 532
Cloud Column Optical Depth Cloud 532 Std	CALIOP Level 2 Cloud Layer	Standard deviation of cloud layer Column Optical Depth Cloud 532.
Cloud Tropopause Altitude	CALIOP Level 2 Cloud Layer	Cloud layer Tropopause Altitude (km).
Cloud Tropopause Altitude Std	CALIOP Level 2 Cloud Layer	Std. dev. cloud layer tropopause altitude (km).
Cloud Tropopause Temperature	CALIOP Level 2 Cloud Layer	Cloud layer Tropopause Temperature (degrees C)
Cloud Column Integrated Attenuated Backscatter 532	CALIOP Level 2 Cloud Layer	Cloud layer Integrated Attenuated Backscatter 532.
Cloud Perpendicular Column Reflectance 532	CALIOP Level 2 Cloud Layer	Cloud layer Perpendicular Column Reflectance 532.
Cloud Parallel Column Reflectance 532	CALIOP Level 2 Cloud Layer	Cloud layer Parallel Column Reflectance 532.
Aerosol Layer Top Altitude	CALIOP Level 2 Aerosol Layer	Aerosol layer level top altitude (km).
Aerosol Layer Top Altitude Std	CALIOP Level 2 Aerosol Layer	Standard deviation of aerosol layer level top altitude (km).
Aerosol Layer Base Altitude	CALIOP Level 2 Aerosol Layer	Aerosol layer level base altitude (km).
Aerosol Layer Base Altitude Std	CALIOP Level 2 Aerosol Layer	Standard deviation of aerosol layer level base altitude (km).
Aerosol Layer Top Pressure	CALIOP Level 2 Aerosol Layer	Aerosol Layer Top Pressure (hPa).
Aerosol Layer Base Pressure	CALIOP Level 2 Aerosol Layer	Aerosol Layer Base Pressure (hPa).

Aerosol Layer Top Temperature	CALIOP Level 2 Aerosol Layer	Aerosol Layer Top Temperature (deg C).
Aerosol Layer Top Temperature Std	CALIOP Level 2 Aerosol Layer	Standard deviation of aerosol Layer Top Temperature (deg C).
Aerosol Layer Base Temperature	CALIOP Level 2 Aerosol Layer	Aerosol Layer Base Temperature (deg C).
Aerosol Layer Base Temperature Std	CALIOP Level 2 Aerosol Layer	Standard dev. of Aerosol Layer Base Temperature (deg C).
Aerosol Midlayer Temperature	CALIOP Level 2 Aerosol Layer	Aerosol MidLayer Temperature (deg C).
Aerosol Midlayer Temperature Std	CALIOP Level 2 Aerosol Layer	Std. deviation of aerosol MidLayer Temperature (deg C).
Aerosol Midlayer Pressure	CALIOP Level 2 Aerosol Layer	Aerosol midlayer pressure (hPa).
Aerosol Lidar Ratio Initial 532	CALIOP Level 2 Aerosol Layer	Aerosol Initial 532 Lidar Ratio (sr).
Aerosol Lidar Ratio Final 532	CALIOP Level 2 Aerosol Layer	Aerosol Final 532 Lidar Ratio (sr).
Aerosol Feature Optical Depth 532	CALIOP Level 2 Aerosol Layer	CALALAY Feature Optical Depth 532.
Aerosol Feature Optical Depth 532 Std	CALIOP Level 2 Aerosol Layer	Std. dev. of aerosol layer Feature Optical Depth 532.
Aerosol Color Ratio	CALIOP Level 2 Aerosol Layer	Integrated Attenuated Total Color Ratio.
Aerosol Integrated Attenuated Backscatter 1064	CALIOP Level 2 Aerosol Layer	Integrated Attenuated Backscatter 1064
Aerosol Integrated Attenuated Backscatter 532	CALIOP Level 2 Aerosol Layer	Integrated Attenuated Backscatter 532
Aerosol Column Optical Depth Stratospheric 1064	CALIOP Level 2 Aerosol Layer	Aerosol layer Column Optical Depth Stratospheric 1064.

Aerosol Column Optical Depth Stratospheric 1064 Std	CALIOP Level 2 Aerosol Layer	Std. dev. of aerosol layer Column Optical Depth Stratospheric 1064.
Aerosol Column Optical Depth Stratospheric 532	CALIOP Level 2 Aerosol Layer	Aerosol layer Column Optical Depth Stratospheric 532.
Aerosol Column Optical Depth Stratospheric 532 Std	CALIOP Level 2 Aerosol Layer	Std. dev. of aerosol layer Column Optical Depth Stratospheric 532.
Aerosol Column Optical Depth Aerosols 1064	CALIOP Level 2 Aerosol Layer	Aerosol layer Column Optical Depth Aerosols 1064.
Aerosol Column Optical Depth Aerosols 1064 Std	CALIOP Level 2 Aerosol Layer	Std. dev. of aerosol layer Column Optical Depth Aerosols 1064.
Aerosol Column Optical Depth Aerosols 532	CALIOP Level 2 Aerosol Layer	Aerosol layer Column Optical Depth Aerosols 532.
Aerosol Column Optical Depth Aerosols 532 Std	CALIOP Level 2 Aerosol Layer	Std. dev. of aerosol layer Column Optical Depth Aerosols 532.

Bibliography

[1] De Boer, G., et al. "Evidence of liquid dependent ice nucleation in high latitude stratiform clouds from surface remote sensors." Geophysical Research Letters 38.1 (2011).

[2] De Boer, G., Tempei H., and G. J. Tripoli. "Ice nucleation through immersion freezing in mixed-phase stratiform clouds: Theory and numerical simulations." Atmospheric Research 96.2 (2010): 315-324.

[3] Haynes, John M., et al. "Rainfall retrieval over the ocean with spaceborne W-band radar." Journal of Geophysical Research: Atmospheres (1984-2012) 114.D8 (2009).

[4] Holz, Robert, et al. "Investigating the Presence of Oriented Ice and Correlations with Precipitation in Mid Latitude Marine Clouds Using Collocated CALIOP, CloudSat, MODIS and Modeling." A proposal submitted in response to National Aeronautics and Space Administration ROSES A.23.

[5] Hu, Yongxiang, et al. "The depolarization-attenuated backscatter relation: CALIPSO lidar measurements vs. theory." Optics Express 15.9 (2007): 5327-5332.

[6] Hu, Y., et al. "CALIPSO/CALIOP cloud phase discrimination algorithm." Journal of Atmospheric and Oceanic Technology 26.11 (2009): 2293-2309.

[7] Hu, Yongxiang. "Depolarization ratio effective lidar ratio relation: Theoretical basis for space lidar cloud phase discrimination." Geophysical research letters 34.11 (2007).

[8] Hu, Yongxiang, et al."Simple relation between lidar multiple scattering and depolarization for water clouds." Optics letters 31.12 (2006): 1809-1811.

[9] King, Michael D., et al. "Cloud and aerosol properties, precipitable water, and profiles of temperature and water vapor from MODIS." Geoscience and Remote Sensing, IEEE Transactions on 41.2 (2003): 442-458.

[10] L'Ecuyer, Tristan S., and Graeme L. Stephens. "An estimation-based precipitation retrieval algorithm for attenuating radars." Journal of applied meteorology 41.3 (2002): 272-285.

[11] Lohmann, U., and Bernd K.. "First interactive simulations of cirrus clouds formed by homogeneous freezing in the ECHAM general circulation model." Journal of Geophysical Research: Atmospheres (1984-2012) 107.D10 (2002): AAC-8.

[12] Lu, M., et al. "The Marine Stratus/Stratocumulus Experiment (MASE): Aerosol cloud relationships in marine stratocumulus." Journal of Geophysical Research: Atmospheres (1984-2012) 112.D10 (2007).

[13] Mitrescu, Cristian, et al. "CloudSat precipitation profiling algorithm-model description." Journal of Applied Meteorology and Climatology 49.5 (2010): 991-1003.

[14] Morrison, H., and J. O. Pinto. "Mesoscale modeling of springtime Arctic mixed-phase stratiform clouds using a new two-moment bulk microphysics scheme." Journal of the atmospheric sciences 62.10 (2005): 3683-3704.

[15] Nagle, Frederick W., and Robert E. Holz. "Computationally efficient methods of collocating satellite, aircraft, and ground observations." Journal of Atmospheric and Oceanic Technology 26.8 (2009): 1585-1595.

[16] Paluch, I. R., and D. H. Lenschow. "Stratiform cloud formation in the marine boundary layer." Journal of the atmospheric sciences 48.19 (1991): 2141-2158.

[17] Petty, Grant William. A first course in atmospheric radiation. Sundog Pub, 2006.

[18] Piironen, P., and E. W. Eloranta. "Demonstration of a high-spectral-resolution lidar based on an iodine absorption filter." Optics letters 19.3 (1994): 234-236.

[19] Platnick, Steven, et al. "The MODIS cloud products: Algorithms and examples from Terra." Geoscience and Remote Sensing, IEEE Transactions on 41.2 (2003): 459-473.

[20] Pruppacher, H. R., J. D. Klett, and P. K. Wang. "Microphysics of clouds and precipitation." (1998): 381-382.

[21] Stocker, T. F., et al. "IPCC, 2013: climate change 2013: the physical science basis. Contribution of working group I to the fifth assessment report of the intergovernmental panel on climate change." (2013)

[22] Tanelli, Simone, et al. "CloudSat's cloud profiling radar after two years in orbit: Performance, calibration, and processing." Geoscience and Remote Sensing, IEEE Transactions on 46.11 (2008): 3560-3573.

[23] Verlinde, J., et al. "The mixed-phase Arctic cloud experiment." Bulletin of the American Meteorological Society 88.2 (2007): 205-221.

[24] Winker, David M., et al. "Overview of the CALIPSO mission and CALIOP data processing algorithms." Journal of Atmospheric and Oceanic Technology 26.11 (2009): 2310-2323.

[25] Wood, R., et al. "The VAMOS ocean-cloud-atmosphere-land study regional experiment (VOCALS-REx): goals, platforms, and field operations." Atmospheric Chemistry and Physics 11.2 (2011): 627-654.

[26] Zhou, Chen, et al. "Study of horizontally oriented ice crystals with CALIPSO observations and comparison with Monte Carlo radiative transfer simulations." Journal of Applied Meteorology and Climatology 51.7 (2012): 1426-1439.

[27] Zuidema, P., et al. "An Arctic springtime mixed-phase cloudy boundary layer observed during SHEBA." Journal of the atmospheric sciences 62.1 (2005): 160-176.